NTNU – Trondheim
Norwegian University of
Science and Technology

Texturing of Lead-free Ferroelectric Ceramics

Eva Rise

Chemical Engineering and Biotechnology
Submission date: June 2013
Supervisor: Tor Grande, IMTE
Co-supervisor: Mari-Ann Einarsrud, IMT
Espen Wefring, IMT

Norwegian University of Science and Technology
Department of Materials Science and Engineering

Declaration

I hereby declare that the work presented in this document has been performed independently and in accordance with the rules and regulations of the Norwegian University of Science and Technology (NTNU).

Trondheim, June 13th 2013

Eva Rise

Preface

This master thesis was written at the Department of Materials Science and Engineering at the Norwegian University of Science and Technology (NTNU) the spring of 2013

First I would like to thank my supervisor Tor Grande for the guidance he has provided during this work. Second I would like to thank the members of the Ferro group for input on texturing, ferroelectricity and results as well as interesting insights into the ongoing research at the department. A special thanks goes to Ph.D. candidate and co-supervisor Espen Wefring for taking the time to answer big and small questions throughout the year. I would also like to thank the technical staff at the department for training me to use the equipment.

Last, but not least I would like to thank my fellow students for good companionship and for making the last five years unforgettable, and my boyfriend for always being there.

Eva Rise

Abstract

The lead-free ferroelectric system $0.75Bi_{0.5}K_{0.5}TiO_3$-$0.25BiFeO_3$ has been investigated with respect to crystallographic texturing. Recent studies have shown that the system have promising electromechanical properties and may be an alternative for replacing lead zirconate titanate (PZT). Texturing was performed on the system with the aim of enhancing the electromechanical properties.

Phase pure $Bi_4Ti_3O_{12}$ templates with aspect ratio of 5.0 were produced. Attempts to convert the $Bi_4Ti_3O_{12}$ templates to plate-shaped $Bi_{0.5}K_{0.5}TiO_3$ in molten salt were unsuccessful. Changing parameters like temperature, salt quantities and holding times did not improve the synthesis, and it was concluded that molten salt synthesis is not suitable for this reaction.

Phase pure $0.75Bi_{0.5}K_{0.5}TiO_3$-$0.25BiFeO_3$ powder was synthesized. Textured ceramics were produced by reactive-templated grain growth, where $Bi_4Ti_3O_{12}$ templates, K_2CO_3 and TiO_2 as precursors were added to a matrix of $0.75Bi_{0.5}K_{0.5}TiO_3$-$0.25BiFeO_3$. Untextured reference samples were made by conventional sintering. Both textured and untextured samples were characterized with respect to phase purity, density, microstructure and ferroelectric properties.

The microstructure of the textured samples was characterized by large pores probably caused by agglomerated precursors prior to sintering. The samples were phase pure and the in-situ conversion of the templates successful. The degree of texture in the textured samples was low due to inadequate orienting of the $Bi_4Ti_3O_{12}$ templates by uniaxial pressing.

Both textured and untextured samples were electrically conductive and thus not exhibiting ferroelectric properties. Further work is needed in order to assess the effect of crystallographic texture on the electromechanical properties of $0.75Bi_{0.5}K_{0.5}TiO_3$-$0.25BiFeO_3$.

Sammendrag

Det blyfri, ferroelektriske systemet $0.75Bi_{0.5}K_{0.5}TiO_3$-$0.25BiFeO_3$ ble undersøkt med tanke på krystallografisk teksturering. Tidligere studier har vist at systemet har lovende elektromekaniske egenskaper og er et mulig alternativ til blyzirconattitanat (PZT). Teksturering av systemet ble gjennomført med mål om å forbedre de elektromekaniske egenskapene.

Det ble produsert faserene $Bi_4Ti_3O_{12}$ templater med sideforhold lik 5.0. Forsøk på å konvertere templatene til plateformet $Bi_{0.5}K_{0.5}TiO_3$ i saltsmelte var mislykkede. Forbedring av syntesen ved endring av parametre som temperatur, saltmengde og holdetid virket ikke. Det ble konkludert med at saltsmeltesyntese ikke er en egnet metode for denne reaksjonen.

Faserent pulver med komposisjon $0.75Bi_{0.5}K_{0.5}TiO_3$-$0.25BiFeO_3$ ble syntetisert. Teksturerte keramer ble produsert ved hjelp av "reactive-templated grain growth", hvor $Bi_4Ti_3O_{12}$ templater, K_2CO_3 og TiO_2 ble tilsatt en matriks av $0.75Bi_{0.5}K_{0.5}TiO_3$-$0.25BiFeO_3$. Uteksturerte referanseprøver ble laget ved hjelp av konvensjonell sintring. Både teksturerte og uteksturerte prøver ble undersøkt med tanke på faserenhet, tetthet, mikrostruktur og ferroelektriske egenskaper.

De teksturerte prøvenes mikrostruktur var preget av store porer som antakelig ble forårsaket av agglomererte reaktanter før sintring. Prøvene var faserene og in-situ konvertering av $Bi_4Ti_3O_{12}$-templatene var vellykket. Teksturingsgraden i de teksturerte prøvene var lav grunnet at enaksiell pressing gav utilstrekkelig orientering av templatene.

Både de teksturerte og uteksturerte prøvene var elektrisk ledende og innehadde dermed ikke ferroelektriske egenskaper. Videre undersøkelser er nødvendig for å bestemme effekten av krystallografisk tekstur på de elektromekaniske egenskapene til $0.75Bi_{0.5}K_{0.5}TiO_3$-$0.25BiFeO_3$

.

List of abbreviations

PZT	Lead Zirconate Titanate, $PbZr_xTi_{1-x}O_3$
BKT	Bismuth Potassium Titanate, $Bi_{0.5}K_{0.5}TiO_3$
BF	Bismuth Ferrite, $BiFeO_3$
BiT	Bismuth Titanate, $Bi_4Ti_3O_{12}$
MSS	Molten Salt Synthesis
CIP	Cold Isostatic Pressing
XRD	X-Ray Diffraction
MPB	Morphotropic Phase Boundary
PPT	Polymorphic Phase Transitions
TGG	Templated Grain Growth
RTGG	Reactive-Templated Grain Growth
BNT	$Bi_{0.5}Na_{0.5}TiO_3$
s/o	Salt to oxide ratio
SEM	Scanning Electron Microscope
SE	Secondary Electron
BSE	Back-Scattered Electron
BKT-BF	$0.75Bi_{0.5}K_{0.5}TiO_3$-0.25 $BiFeO_3$

Table of Contents

1 Introduction

1.1 Motivation

The piezoelectric effect, a material's ability to develop electric polarization when subject to mechanical stress, was discovered in 1880 by Jacques and Pierre Curie. The effect was discovered in Rochelle salt and found in single crystals like quarts and tourmaline [1]. In the 1940s, it was discovered that the high dielectric constant of $BaTiO_3$ was due to its ferroelectric nature and that domains within polycrystalline ceramics could be oriented by an external electric field and remain reoriented after the electric field was turned off. Since then, piezoelectric and ferroelectric single crystals and ceramics has found many applications, like in electronic devices like sensors, actuators and transducers [2] as well as capacitators, memory (FeRAM) and electro-optics [1].

Lead zirconate titanate, $PbZr_xTi_{1-x}O_3$ (PZT), is a common ceramic material [3]. It is very versatile and can be tailored to fit many applications, as it possesses high d_{33} coefficients and Curie temperatures. However, PZT contains large amounts of lead, which is toxic. Lead oxide is released during production and waste disposal [2]. Directives issued by the European Union [4, 5] restricts the use of lead and other hazardous substances, and states that use of PZT will be prohibited as soon as a good replacement is available. Consequently, the interest and research for lead-free ceramics has bloomed.

There are several ways to engineer lead-free piezo- and ferroelectric ceramics with high performance, i.e. compositional and structural engineering [6]. Texturing is an example of a structural engineering technique [7]. This process controls the microstructure during sintering and produces polycrystalline ceramics with grains oriented in the same direction, striving to achieve properties comparable to those of single crystals.

Bismuth based materials are very attractive as alternatives to PZT mainly because of the non-toxicity of bismuth, but also of its availability and low cost [2]. Both bismuth potassium titanate (BKT) and bismuth ferrite (BF) have been investigated as alternatives, but have shown moderate piezoelectric and structural properties and are difficult to sinter [8]. A few studies have been made on mixtures between BKT and BF and for certain compositions promising results have been shown [8-12]. The system needs to be studied more thoroughly. If it is possible to texture BKT-BF mixtures, they may be a candidate for replacing PZT.

1.2 Aim of work

The aim of this thesis is to prepare textured lead-free ferroelectric ceramics of the material system $0.75Bi_{0.5}K_{0.5}TiO_3$-.$0.25BiFeO_3$. The material and its precursors will be characterized with respect to morphology, microstructure and composition as well as density and ferroelectric performance. The textured materials will be characterized with respect to degree of texture and compared with non-textured reference materials. This thesis is a continuation of the author's specialization project "Synthesis of bismuth titanate templates for tape casting of textured lead-free ferroelectric ceramics" as part of the Specialization course TMT4500 the autumn of 2012.

2 Background

2.1 Piezoelectricity and ferroelectricity

2.1.1 Piezoelectricity

Piezoelectricity is the development of polarization, and therefore a measurable electrical charge, in a material as a consequence of an applied mechanical stress [1]. This is called the direct piezoelectric effect. The converse piezoelectric effect involves volume expansion or contraction of the material when exposed to an electric field. This is illustrated in Figure 2.1.

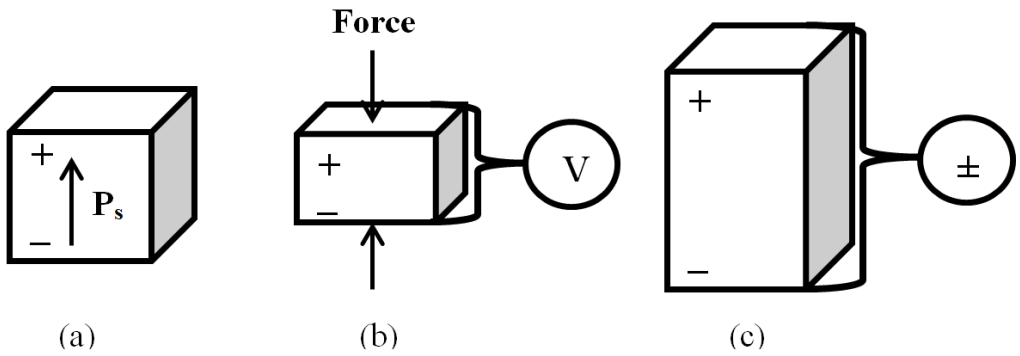

Figure 2.1: Illustration of the piezoelectric effect; (a) Material in its original state with spontaneous polarization P_s indicated; (b) The direct piezoelectric effect, where a mechanical force creates a measurable electrical charge; (c) The converse piezoelectric effect, where the material volume expands as a response to an applied voltage of the same sign as the polarization.

Mathematically, piezoelectricity can be described by the following equations [13]:

$$P = d\sigma \text{ (direct effect)} \quad (2.1)$$

$$\varepsilon = dE \text{ (converse effect)} \quad (2.2)$$

where P represents electric polarization, σ mechanical stress, ε stands for mechanical strain, E the strength of the electric field and d is the piezoelectric coefficient which correlates the stimuli with the response. The piezoelectric coefficient is numerically identical for both the direct and converse effect, but is denominated differently. The direct effect is denominated by [pC/N] and the converse by [pm/V]. Piezoelectricity is a directional property, which means the effects are anisotropic and varies with the crystallographic direction. Equations 2.1 and 2.2 are thus not sufficient to describe the piezoelectric effects. The equations above can instead be expressed as a three-axis system, where tensile stress and strain (σ and ε, respectively) are expressed by the numbers 1, 2 and 3 along the x, y and z axes, respectively, and shear stress and strain are denoted by 4, 5 and 6, normal to the x, y and z axes [13]. This is illustrated in Figure 2.2. Alternative equations are given in equations 2.3 and 2.4.

$$P_i = d_{ij}\sigma_j \qquad (i = 1, 2, 3, j = 1, \ldots, 6) \qquad (2.3)$$

$$\varepsilon_j = d_{ij}E_i \qquad (i = 1, 2, 3, j = 1, \ldots, 6) \qquad (2.4)$$

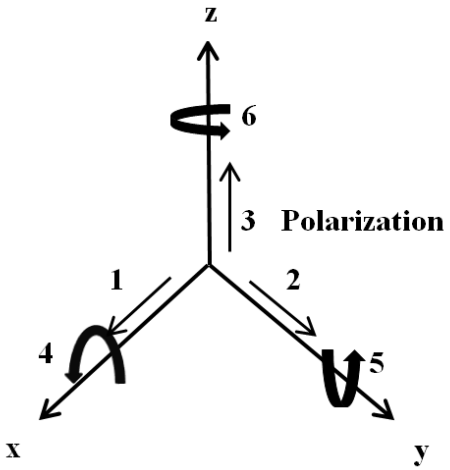

Figure 2.2: Illustration of subscripts used in equations 2.3 and 2.4. Tensile components are denoted by 1, 2 and 3 along the x, y and z axis, while shear components are denoted by 4, 5 and 6 about the x, y and z axes.

It should be noted that all materials undergo a small dimensional change when exposed to an electric field [14]. If the strain is proportional to the square of the electric field, the effect is said to be electrostrictive. If the material shows a linear proportionality between the field and the shape change, the material is piezoelectric.

The piezoelectric coefficient, d_{33}, describes how the polarization and tensile stress develop along the 3 axis. $S_{3,max}/E_{3,max}$ is a quantity similar to the piezoelectric coefficient, with the difference that it includes strain contributions by domain switching [2].

The directionality of the piezoelectric effect results in certain symmetry requirements. Symmetry around a point in space is described by symmetry elements; a center of symmetry, axes of rotation, mirror planes and combinations of the three already mentioned elements. Using these elements, all materials can be divided into 32 different point groups. A criterion for being piezoelectric is the lack of a centre of symmetry [13], reducing the possible crystal classes down to 20.

2.1.2 Ferroelectricity, domains and poling

Pyroelectric crystals represent a subgroup of piezoelectric crystals, containing the 10 crystal classes with a unique polar axis. Pyroelectric crystals develop or alter an existing spontaneous electric polarization when the temperature changes. Ferroelectric crystals are a subgroup of pyroelectrics. A ferroelectric material also develops spontaneous polarization, but the direction of the polarization is reversible by application of an electric field. An important difference between pyro- and ferroelectricity is that pyroelectricity rests on symmetry conditions while ferroelectricity must be empirically confirmed [3]. The relationship between the piezo-, pyro- and ferroelectrics and their crystallographic requirements are illustrated in Figure 2.3. Piezoelectric crystals that are not pyro- or ferroelectric lose their polarization

when the stress is no longer applied. Thus, in many applications only ferroelectric piezoelectrics can be applied. Ferroelectricity is found in several structures, i.e. perovskites and bismuth layered structures, the most common and industrially important being the perovskite structure.

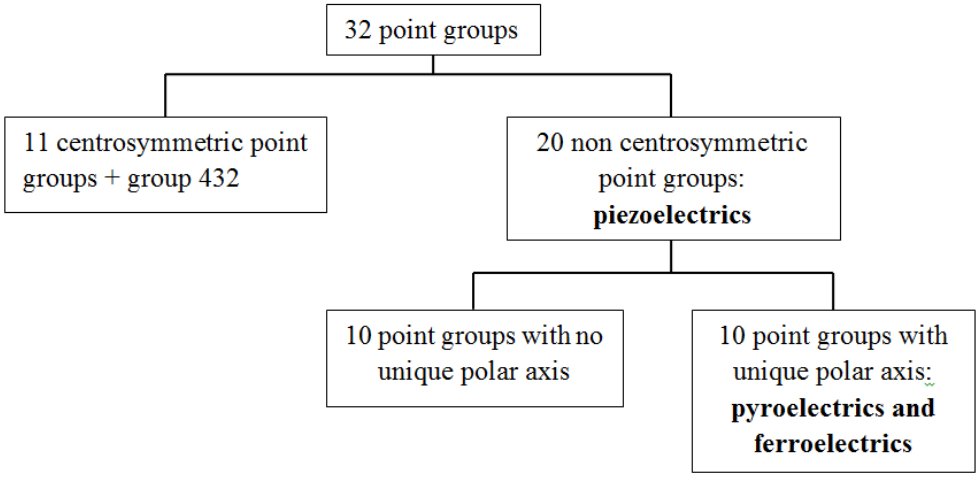

Figure 2.3: Point group requirements for piezoelectric and ferroelectric ceramics. Figure redrawn from Tilley [15].

A polycrystalline ceramic consists of multiple grains. These grains are mostly randomly oriented, which means that the polar axes of the crystals also are randomly oriented. This means that even though each individual grain itself is piezoelectric, the net polarization is zero. Thus, the ceramic behaves non-piezoelectrically.

Domains are regions within the material where the direction of the spontaneous polarization in the material is uniform [14]. To minimize the energy associated with the spontaneous polarization, oppositely polarized domains arise, separated by domain walls. Domain walls are regions where the polarization switches direction. Domain walls between oppositely directed domains are called 180° domain walls.

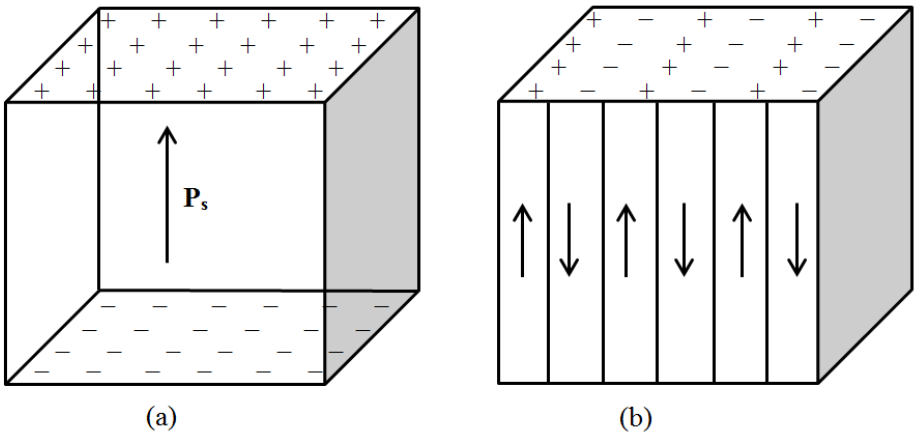

Figure 2.4: Schematic of domain formation in ceramics; (a) A single domain with the direction of spontaneous polarization P_S marked; (b) Formation of 180° domains to minimize energy. Adapted from Moulson & Herbert [14].

Poling is the process of transforming the multidomain state to a single domain by applying an external electric field [14]. Domains with polar moment well aligned with the direction of the field will grow at the expense of poorly aligned domains, creating a net polarization in the ceramic. When all the domains are aligned, the saturation polarization, P_{sat}, has been reached. The process of poling involves movement of the domain walls. When non-180° domain walls move, the physical dimensions of the grain changes. This causes a strain in the material. The strain causes some of the domains to switch back when the electric field is removed, leaving a remnant polarization in the ceramic, P_R. The electric field required to switch net polarization direction is called the coercive field, E_C. The Curie temperature, T_C, marks a ferro- to paraelectric phase transition [14]. By heating the material above the T_C, the net polarization switches back to zero. The depolarization temperature, T_d, though not universally defined, is proposed defined as the temperature where the rate of loss of remnant polarization is highest [16, 17]. This temperature often coincides with the T_C, but can also occur at lower temperatures. The ferroelectric behavior can be graphically described by a hysteresis loop, illustrated in Figure 2.5.

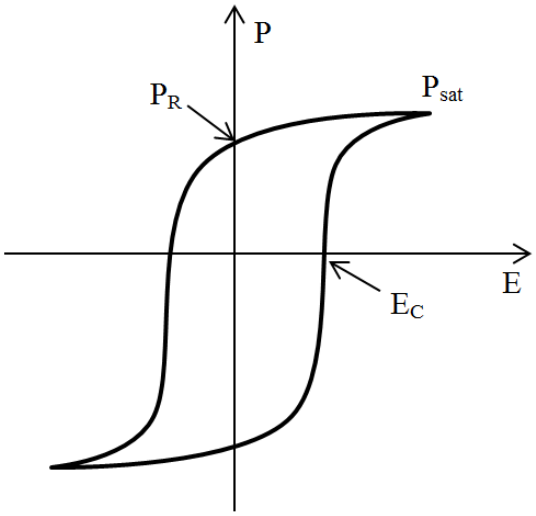

Figure 2.5: Schematic of a typical hysteresis loop of a ferroelectric material, showing polarization as a function of applied electric field.

2.2 Perovskites and bismuth layered structures

2.2.1 The Perovskite structure

As previously mentioned, perovskite structured ferroelectrics are the industrially most important. The general formula of the perovskite structure is ABX_3 [18]. X typically represents oxygen ions, O^{2-}, while A and B are cations whose added oxidation states equals +6. The perovskite structure can be regarded as a framework structure with corner sharing BX_6 octahedras, in which the A cations are placed in the twelve-coordinate interstices. The ideal cubic structure is shown in Figure 2.6. Misfitting A or B cations give rise to distortions of the structure to lower symmetry, i.e. tilting of the BO_6 octahedras or off-centering of the B cations. Figure 2.7 illustrates tetragonal distortion of the perovskite structure, with off-centered B cations. The ability of the perovskite structure to adapt to such distortions makes it very tolerant to different compositions.

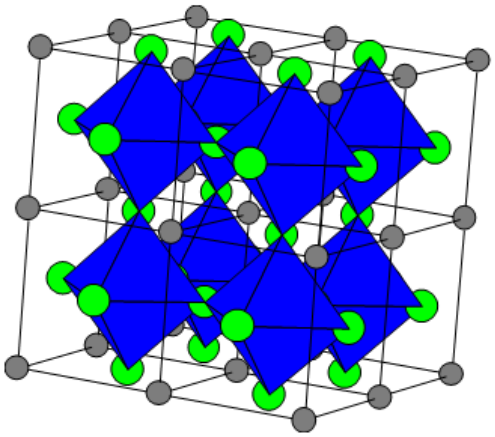

Figure 2.6: The unit cell of the ideal cubic perovskite. The A cations are represented with grey dots, X anions with green dots and the B cations are situated inside the blue octahedras. Figure from López-Juárez et al. [19].

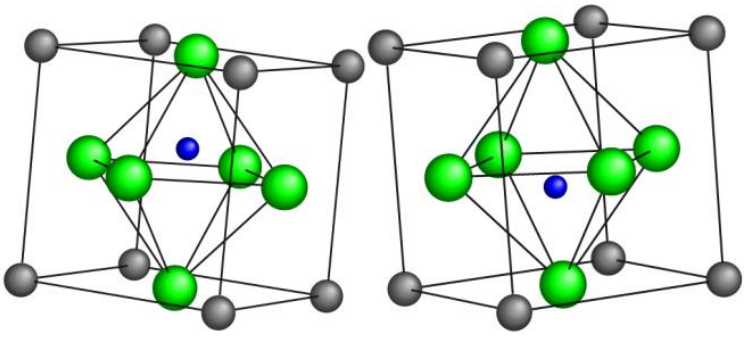

Figure 2.7: Tetragonal distortion of the perovskite structure, with the two possible polarization states depicted. Figure from López-Juárez et al. [19].

2.2.2 The Aurivillius structure

Aurivillius phases were first described by Bengt Aurivillius in 1950 [20]. The general formula of Aurivillius phases is $A_{m-1}Bi_2B_mO_{3m+3}$ and they consist of alternating layers of pseudo-perovskite blocks with composition $(A_{m-1}B_mO_{3m+1})^{2-}$ and fluorite-like bismuth oxygen layers with composition $(Bi_2O_2)^{2+}$. Here A represents mono-, di- or trivalent cations, B represents cations with a valency of 3, 4 or 5 and m denotes the number of perovskite layers. Fractional values of m occur in compounds with perovskite layers of alternating thickness. In the case of $Bi_4Ti_3O_{12}$ (BiT), m = 3, A = Bi^{3+} and B = Ti^{4+}. The structure is shown in Figure 2.8. BiT particles with highly anisometric morphology can be synthesized with molten salt synthesis (MSS) [21], due to the layered crystal structure giving preferential growth in the ab-plane.

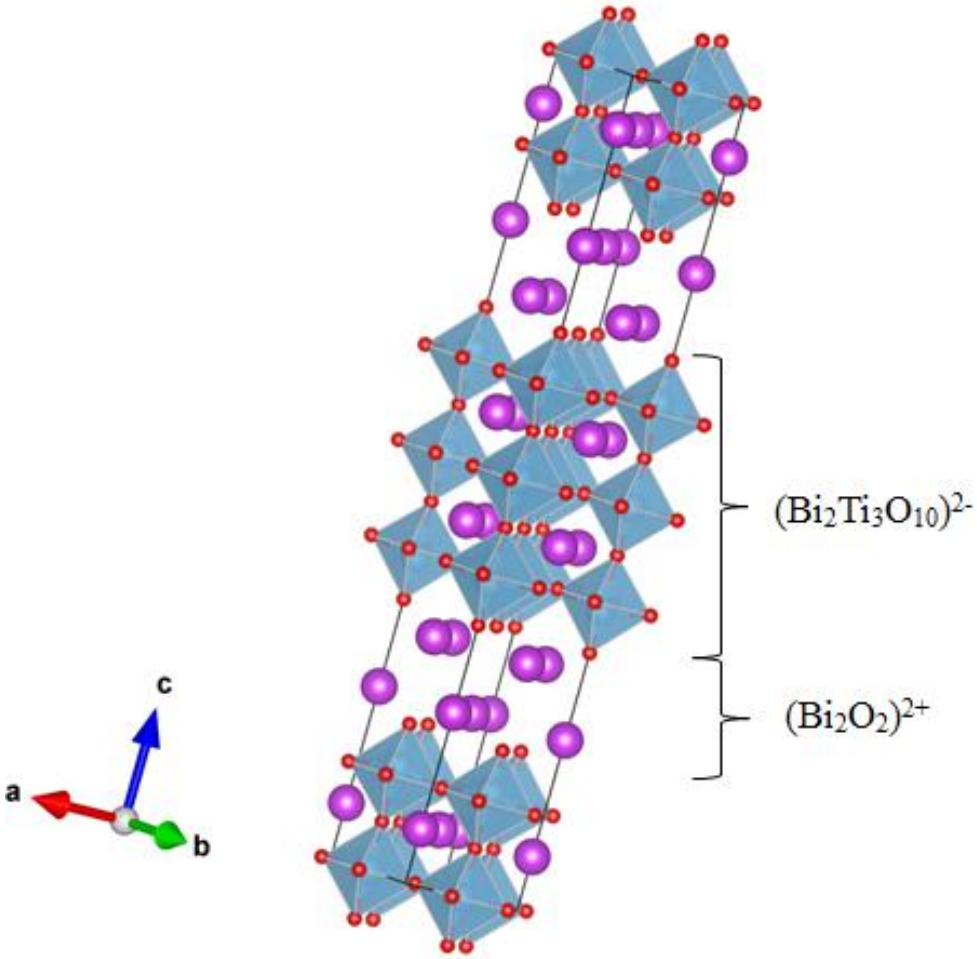

Figure 2.8: The Aurivillius structure, illustrated with BiT.

2.3 Bismuth potassium titanate – bismuth ferrite

Bismuth based materials are attractive alternatives to PZT-based ferroelectrics due to their nontoxicity and availability of their raw materials [2]. Bismuth potassium titanate, $Bi_{0.5}K_{0.5}TiO_3$ (BKT), is a tetragonally distorted lead-free ferroelectric perovskite. It was first synthesized in 1957, but its ferroelectricity was discovered in 1962 [22]. It exhibits a second phase transition to pseudo-cubic structure just above 300 °C and has a T_c of >370 °C. Pure BKT does not have suitable properties for application as it is hard to sinter [23] and have a high E_c, making it difficult to pole. Instead BKT has marked itself as an important end compound for various solid solutions.

Bismuth ferrite, $BiFeO_3$ (BF), is a rhombohedrally distorted ferroelectric perovskite with relatively low dielectric and piezoelectric properties. It has a T_c of >820 °C and has, like BKT, been proven hard to prepare. However, the interest in considering its piezoelectric potential in lead-free applications has been renewed as the compound is multiferroic at room temperature [24] and exhibits a very high strain response under high electric field amplitudes [25, 26]. Selected properties of BKT and BF are summarized in Table 2.1.

The (1-x)BKT-xBF system has not yet been thoroughly studied, perhaps due to the moderate piezoelectric properties of BKT and BF, but a few works have investigated the system with respect to electric and structural properties [8]. Kim et al. [10] have studied the system in the range $0 \leq x \leq 0.4$, while Matsuo et al. [12] have investigated the range $0.4 \leq x$ 0.8. Morozov et al. [9] have conducted a study in the range $0.1 \leq x$ 0.9 in order to find the composition exhibiting the highest dielectric and electromechanical properties in the system and a preliminary characterization of the ceramic displaying the highest electromechanical performance [8].

Two phase boundaries have been suggested upon moving from BKT to BF [8-12]: one between the tetragonal phase and a pseudocubic phase at $x \approx 0.25$, and one separating a pseudocubic phase and the rhombohedral phase at $x \approx 0.6$. According to Morozov et al. a clear maximum in piezo- and ferroelectric performance and relative dielectric permittivity (ε_r) is found at $x \approx 0.25$. However, the piezoelectric properties around $x \approx 0.6$ are ambiguous, as some properties showed a pronounced maximum at the phase boundary (E_c, P_R and d_{33}) while others did not (S_{max}/E_{max} and ε_r).

Table 2.1: A selection of piezoelectric properties of BKT and BF.

Material system	T_c	ε_r	d_{33}	S_{max}/E_{max}
BKT [2]	>370 °C	770	80-100 pC/N	130 pm/V
BF	>820 °C [27]	30 [28]	50-70 pm/V [29]	117 pm/V [30]

2.4 Engineering to increase properties

2.4.1 General

There are different methods of enhancing the electromechanical response in piezoelectric materials. Compositional engineering is the traditional method, in which a material's composition is optimized by being brought close to morphotropic phase boundaries (MPB) or polymorphic phase transitions (PPT) [6]. MPBs mark abrupt structural changes with variation in composition [3] where properties like dielectric permittivity and piezoelectric coefficient reach their maximums [2]. PPTs mark similar structural instabilities with temperature [6].

Another approach is structural engineering, which focuses on the microstructure of a piezoelectric material. Structural engineering techniques include grain size optimization, domain engineering and texturing, the latter being utilized in this work. The advantage of texturing compared to compositional engineering is that there are no negative effects like lowered T_d [2].

2.4.2 Texturing

Crystallographic texturing is the process of producing dense, polycrystalline ceramics with nonrandom distribution of grain orientations by addition of templates (large, anisometric particles) to a uniaxial matrix. This nonrandom distribution of grain orientations enhances the ferroelectric response and elevates the properties of the material [7]. The goal of texturing is to make polycrystalline ceramics with properties comparable to those of single crystalline ceramics. This is illustrated in Figure 2.9.

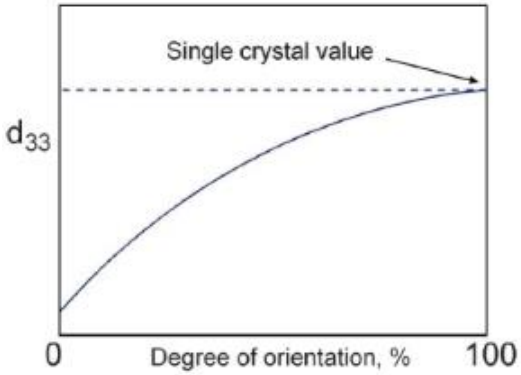

Figure 2.9: Ferroelectric coefficient as a function of degree of orientation. Figure from Leontsev & Eitel [6].

The anisotropy of a material on a microscopic level is connected to the macroscopic anisotropy of the material [31], as illustrated in Figure 2.10. Ferroelectrics have only two antiparallel domain states available [7]. In a polycrystalline ceramic the grains are oriented in different directions, which make poling harder as some grains do not have possible domain states aligned or close to aligned with the electrical field. These grains will not be able to switch domain states and may even block switching of neighboring grains. Texturing is a way of orienting these grains, to make poling easier and the piezoelectric response higher.

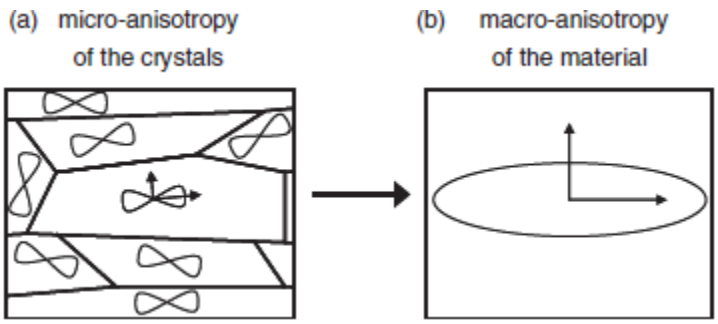

Figure 2.10: The connection between the (a) micro-anisotropy of crystalline grains and the (b) macro-anisotropy of a textured material. Figure from Jones et al. [31].

2.4.2.1 Templated grain growth and reactive-templated grain growth

Templated grain growth (TGG) uses a minority of large, anisometric single crystals (templates) in a relatively fine, equiaxed matrix powder to control the microstructure of the ceramic during sintering [7]. The templates are oriented in the matrix during green body forming, typically tape casting or extrusion, and grow at the expense of the smaller matrix particles (Ostwald ripening) during sintering.

In reactive-templated grain growth (RTGG) the matrix acts as a precursor to the final ceramic phase [7]. In this process, the templates act as nucleation sites for the transformation and seed the phase transition. Anisometric particles with simpler composition and easier fabrication routes than the target material are used [32]. These particles are aligned in the matrix and converted to the target material during sintering while the morphology of the template is maintained. Figure 2.11 shows a schematic of the RTGG process.

One of the main differences between TGG and RTGG is that in the TGG process heteroepitaxial growth usually takes place on the template, while in the RTGG process is topotactic and the single crystallinity of the template does not change during the process [33].

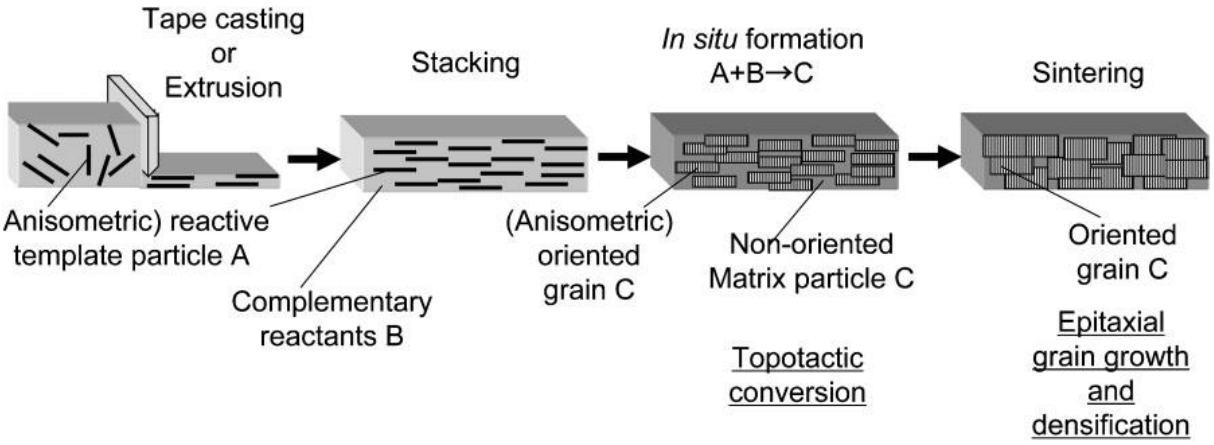

Figure 2.11: The process of RTGG. The TGG process lacks the third step (topotactic conversion), but is otherwise the same as RTGG. Figure from Tani et al. [32]

2.4.2.3 Template selection and quality of the textured material

The preferred growth of the template particles is dependent on the crystallographic and thermal properties of the template particles compared to the matrix particles as well as thermodynamic and kinetic conditions favoring template growth [7, 34]. The template and the product phase must have epi- or topotaxial lattice matching (2D and 3D lattice matching between nucleus and substrate, respectively) with respect to each other. The lattice parameter should not mismatch more than 15 %. The minimum size ratio between the templates and matrix powder to thermodynamically sustain template growth is ~1.5, but a higher ratio is preferable due to kinetic considerations. It is important that the overall reaction does not include intermediate phases that can disturb the crystallographic similarity between the template and the product phase. To obtain preferred growth of the template particles, the material must be denser than 95 % [7]. This is because pores restrain boundary motion and the large template particles inhibit densification. Once 95 % density is achieved, the template growth is rapid.

The degree of texture is quantified as the Lotgering factor, f, which is calculated as follows [35]:

$$f = \frac{P - P_0}{1 - P_0} \tag{2.5}$$

$$P = \frac{\sum I_{(00l)}}{\sum I_{(hkl)}} \tag{2.6}$$

$$P_0 = \frac{\sum I_{0(00l)}}{\sum I_{0(hkl)}} \tag{2.7}$$

I is the intensity of a diffraction line in the textured sample pattern and I_0 the intensity of the corresponding peak in a randomly oriented sample. For an ideally oriented material, all (*h k l*) reflections except the (*0 0 l*) reflection vanish from the diffractogram when X-ray beams are reflected from planes parallel to the material's basal plane. In the X-ray diffractograms of non-ideally oriented samples, the (*h k l*) diffraction lines still occur. The ratio between the (*0 0 l*) and (*h k l*) intensities increases with improving orientation. Hence, the Lotgering factor will be a number between 0 and 1, where 0 corresponds to no orientation and 1 corresponds to complete orientation in the sample. The Lotgering factor does not describe the distribution of the orientation, but is considered an estimate of the volume fraction of textured material.

2.5 Ceramic synthesis

2.5.1 Solid state synthesis, calcining, pressing and sintering

Solid state synthesis is a common way of producing ceramic powders. The method involves mixing and heating of two or more non-volatile solids below their melting temperatures. The solids react and form the desired product [36]. High temperatures, typically between 500 and 2000 °C, are often required. The reactions are commonly slow, but increasing the temperature increases the diffusion rate of the reactants. The reaction rate is often controlled by the rate of diffusion of the slowest species [15]. Due to the remaining reactants becoming increasingly separated from each other throughout the process, it can be difficult for solid state reactions to go to completion [18]. Because of this, the reactants must be ground to small particle sizes and well mixed to increase reactivity and minimize the distance the reactants have to diffuse. It is common to grind, remix and heat treat the partially reacted mixtures to bring new reactant surfaces in contact with each other.

Calcining refers to high-temperature treatment of a powder to modify the characteristics of the powder, i.e. decomposition and reaction [37]. Gases are often evolved during these modifications and calcining is performed prior to consolidation to avoid buildup of gases that can cause cracks.

Uniaxial pressing involves consolidation of powder into a die and shaping the green body by applying pressure along a single axial direction [37]. Problems associated with uniaxial pressing include cracking and density variations. Density variations may be due to non-uniform filling of the die or the presence of hard agglomerates in the powder. The hard agglomerates can shield the surrounding powder from exposure to maximum pressure or trap porosity. The agglomerate may then shrink more than the adjacent powder during densification and leave a pore.

Sintering is the process of removing pores, producing intergrowth and strong bonding between adjacent particles [37]. In short terms, sintering is the densification process of a ceramic. The process can be divided into three stages, illustrated in Figure 2.12. The first stage involves particle rearrangement and beginning neck formation at points of contact between the particles. The second stage, or the intermediate sintering stage, is when most of the shrinkage occur. The size of the necks between the particles increases, the porosity decreases and the particles move closer together. Some grains begin to grow at the expense of others due to grain boundary movement. The third and final stage involves removal of the final porosity by vacancy diffusion along the grain boundaries. The final stage is when the rate of grain growth is highest. Grain growth is driven by reduction of the surface energy. Thus, the sintering process is affected by temperature, particle size, uniformity of the particle packing and particle size distribution. It is important to have as fine particles as possible, as this give more rapid sintering at lower temperatures. Agglomerated particles and too narrow size distributions give less uniform packing, and must be avoided.

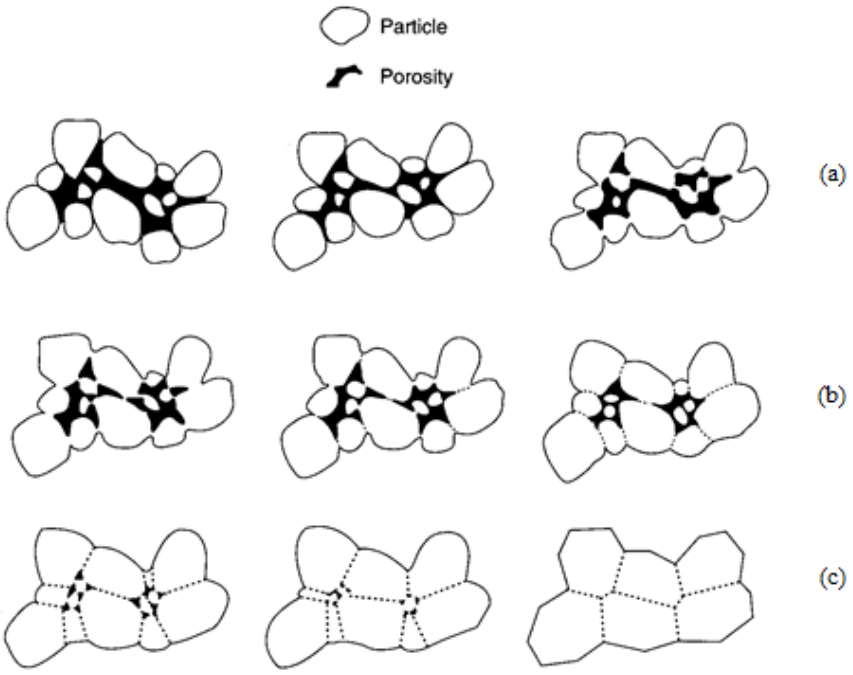

Figure 2.12: The three stages of the sintering process; (a) Initial stage with neck formation and particle rearrangement; (b) Intermediate stage with high increase in density; (c) Final stage with removal of final porosity and grain growth. Figure from Richerson [37].

2.5.2 Molten salt synthesis

The molten salt synthesis (MSS) method generally has two main purposes; preparation of powders for sintering and preparation of anisometric single crystals, the latter being the objective of this work. In MSS salt with a low melting point acts as a solvent for the oxides involved and is used to control characteristics and properties of the powder [38]. The molten salt has multiple advantages. It increases the reaction rate due to increased diffusion rate of reactants and products and lowers the reaction temperature compared to a solid state synthesis. It increases the homogeneity and controls the degree of agglomeration as well as the particle size and shape.

The procedure is as follows: a mixture between the reactants and salt is heated above the melting point of the salt. The salt melts and the product particles are formed with properties controlled by selection of the heat treatment conditions. After the heat treatment the salt is removed with an appropriate solvent, typically water.

The amount of salt affects the synthesis, and is typically between 80 – 120 wt% of the reactant mixture. There must be enough salt to completely cover the particle surfaces and interstices. Without enough salt, full effect of the liquid phase will not be obtained. Neither is excessive amounts of salt beneficial as it can cause separation of reactant particles, which leads to reduction of the reaction rate.

The particle formation can be divided into two separate stages: the reaction stage and the growth stage. In the reaction stage, reactants dissolve and react to form product particles. In the growth stage all reactant particles have been consumed, and large particles increase their

size at the expense of small particles through Ostwald ripening. The final particle size is determined by temperature and time, as the growth is controlled by solubility and diffusion of the product in the salt flux. The growth of non-centrosymmetric systems like tungsten-bronze or perovskite layered structures is anisotropic, as the symmetry of a crystal's internal structure is reflected in the symmetry of its external properties, resulting in highly facetted grains [7], i.e. the plate-shape exhibited by Aurivillius phases.

2.6 Topochemical conversion

Topochemical conversion, also referred to as "soft chemistry" [39], refers to manipulation of an existing structure while maintaining principal features [40]. Topochemical manipulation includes a number of reactions, like ion exchange, substitution, intercalation and layer construction. Topochemical conversion is a powerful tool to obtain thermodynamically inaccessible structural and morphological features by stabilizing structures at a kinetic level, like producing plate shaped particles of compounds with a cubic or pseudo-cubic crystal structure. During conversion most of the bond connectivity in the precursor phase is preserved, ensuring that the structure of the final phase closely resembles the structure of the starting material [39]. The reactions must be executed at temperatures low enough to avoid extensive amounts of bond breaking and rearrangement of the structural framework.

The difference between topochemical conversion and epi/topotactical growth must be emphasized. Epi/topotactical growth involves heterogeneous nucleation and growth on the particle surface, while topochemistry involves a change in the existing particle. The growth is referred to as epitactic if the similarity between the nucleus and the substrate is restricted to the 2D interface between them [18]. If the structural similarity extends to 3D, the process is referred to as topotactic.

The conversion of BiT to $Bi_{0.5}Na_{0.5}TiO_3$ (BNT) and $Bi_{0.5}(Na_{0.87}K_{0.13})TiO_3$ has been successfully performed and examined by several scientists [41-44]. The transformation is believed to be topochemical (ion exchange) rather than epitaxial [44], where Na and K ions diffuse into the structure. To the best of the author's knowledge, a conversion to BKT has not yet been successfully performed.

3 Experimental work

3.1 Synthesis of $Bi_4Ti_3O_{12}$ templates

$Bi_4Ti_3O_{12}$ platelets with Aurivillius structure were synthesized by MSS. TiO_2 (Aldrich, 99.9%) and Bi_2O_3 (Aldrich, 99.9%) were used as raw materials. KCl (Alfa Aesar, 99.997%) was used for the molten salt flux.

The raw materials were crushed and mixed by mortar and pestle. The mixtures were placed in an alumina crucible covered with an alumina disk to hinder evaporation of volatile species. The samples were heated to 1100 °C for a time range of 0 – 2 hours with heating rates of 180 – 250 °C/h. The mixtures were washed with hot distilled water to dissolve the salt flux after the heat treatment. Finally, the products were dried and characterized.

3.2 Conversion of $Bi_4Ti_3O_{12}$ templates to $Bi_{0.5}K_{0.5}TiO_3$

$Bi_{0.5}K_{0.5}TiO_3$ templates with perovskite structure were synthesized in molten KCl (Alfa Aesar, 99.997%). Previously synthesized $Bi_4Ti_3O_{12}$ platelets, K_2CO_3 (Sigma-Aldrich, 99.99%) and TiO_2 (Aldrich, 99.9%) were used as precursors. Varying amounts of KCl was used for the molten salt flux, with a weight ratio range of 1 – 4 between salts and oxides (s/o).

The precursors were dried in vacuum at 200 °C to remove water from hygroscopic species, then mixed in a ball mill with zirconia balls for 24 hours and placed in an alumina crucible covered with an alumina disc to avoid evaporation of volatile species. The samples were heated to 900 – 1000 °C and held there for 2 – 4 hours. The templates were washed with hot distilled water to dissolve the KCl flux after the heat treatment. The products were then dried and characterized.

3.3 Production of $0.75Bi_{0.5}K_{0.5}TiO_3$-$0.25BiFeO_3$ powder

$0.75Bi_{0.5}K_{0.5}TiO_3$-$0.25BiFeO_3$ (BKT-BF) powder was prepared through solid state synthesis. Bi_2O_3 (Aldrich, 99.9 %), TiO_2 (Aldrich, 99.9 %), K_2CO_3 (Sigma-Aldrich, 99.99 %) and Fe_2O_3 (Aldrich, 99.999 %) were used as precursors.

The precursors were dried in vacuum at 200 °C to remove water from hygroscopic species, weighed, crushed and homogenously mixed through ball milling using zirconia balls and isopropanol for 18 – 24 hours. The mixture was dried, sieved through a 250 μm mesh and calcined in air at 800 °C for 5 hours. After the initial calcination, the powder was remilled in isopropanol for 24 hours and recalcined in air at 860 °C for 5 hours. The powder was remilled in isopropanol for 24 hours, then dried and sieved through a 250 μm mesh.

3.4 Production of ceramic samples

Untextured ceramic samples were produced by uniaxially pressing the previously produced BKT-BF powder into pellets, then cold isostatic pressing (CIP) at 200 MPa and sintering in air at 1080 – 1100 °C for 2 – 10 hours, following the sintering program shown in Figure 3.1.

Ceramic samples of textured BKT-BF were made by RTGG. The BKT-BF powder was mixed with 0 – 10 wt% $Bi_4Ti_3O_{12}$ (BiT) templates, TiO_2 (Aldrich, 99.9 %) and K_2CO_3 (Sigma-Aldrich, 99.99 %). The templates were oriented and the green body shaped by uniaxially pressing the precursors to pellets, then cold isostatic pressing at 200 MPa. The pellets were sintered in air at 1080 – 1100 °C for 10 hours following the sintering program shown in Figure 3.1.

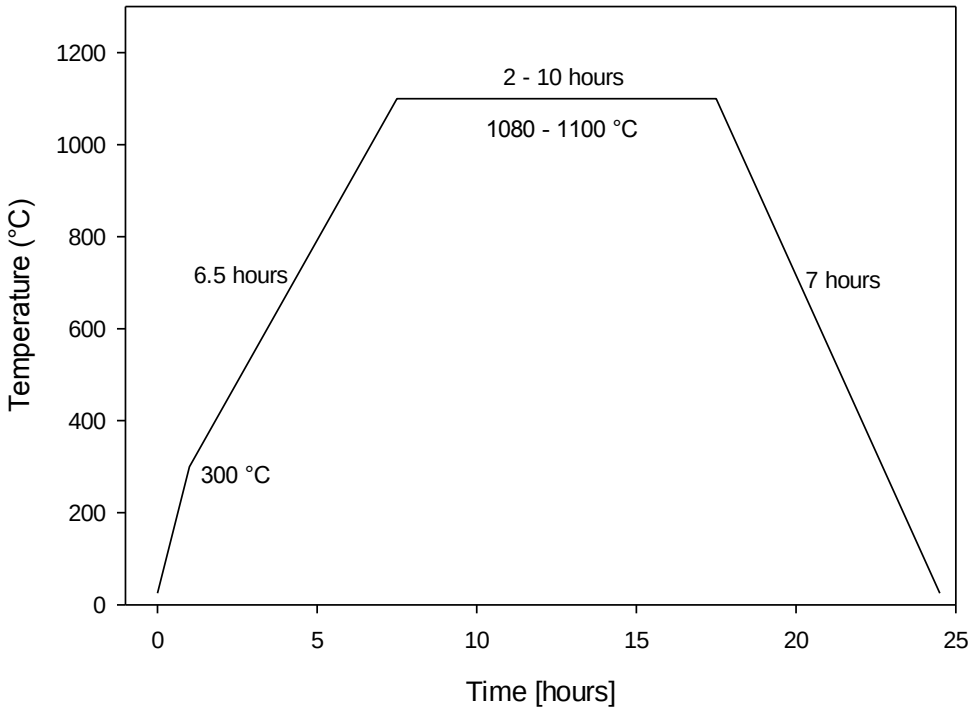

Figure 3.1: Sintering program of the ceramic samples.

3.5 Structural characterization

X-ray diffractograms were recorded with a Bruker Focus D8 with CuKα-radiation using 0.014 2θ steps with a counting time of 0.75 seconds per step from 15° 2θ to 80° 2θ. Ceramic samples were rotated during recording. A 0.2 mm slit was used. Powdered samples were prepared by conventional top filling.

The Lotgering factor of the textured samples was calculated from the obtained X-ray diffractograms as described in chapter 2.4.2.2. Samples were prepared by dispersion in ethanol and casting on a single crystal sample holder. Separation of templates from agglomerates for investigation by X-ray diffraction was performed by dispersion in ethanol,

sedimentation of the agglomerates, then decanting of the remaining dispersion and subsequently drying on a single crystal sample holder.

The BiT and BKT template size and morphology were investigated with a Hitachi S-3400N LVSEM. The templates were dispersed in ethanol and dried on an aluminum stub used for examination. Prior to the examination, the samples were coated with carbon to make them electrically conductive. The particle size of the BiT template particles was found as the diameter of the platelets. 20 particles per sample were measured and average particle size was calculated. Micrographs were taken in both the secondary electron (SE) and back-scattered electron (BSE) regime.

Fracture surfaces of the sintered ceramics were investigated with a Hitachi S-3400N LVSEM to examine the microstructure of the samples. The ceramics were fractured parallel to the uniaxial pressing direction and micrographs taken normal to the pressing direction, as illustrated in Figure 3.2. Prior to the examination, the samples were coated with carbon to make them electrically conductive.

The densities of the sintered samples were determined by the Archimedes method in accordance with ISO 5017:1998 with isopropanol as immersion liquid.

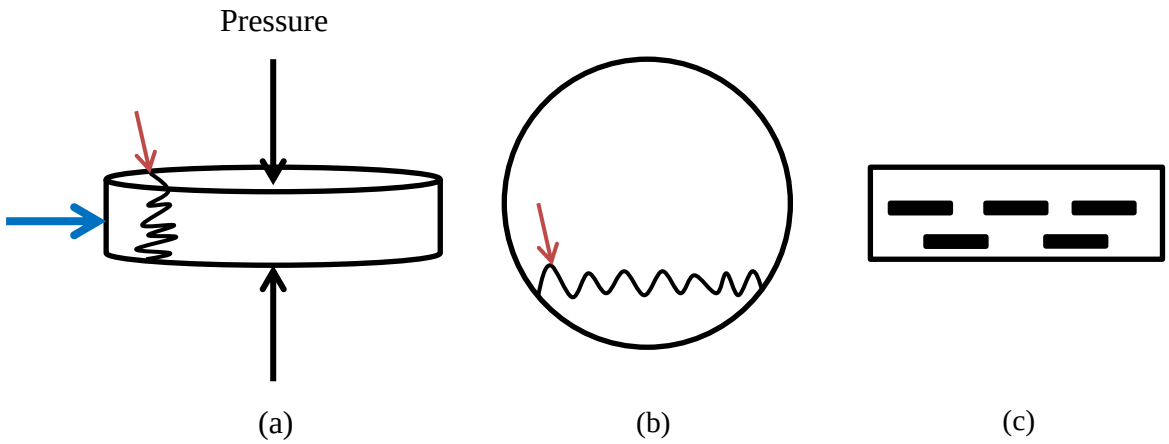

Figure 3.2: Schematic of fracture surfaces; (a) Pellet viewed from the side, with the direction of uniaxial pressing marked with black arrows. Red arrow points towards the fracture, blue arrow indicates the view of the SEM micrographs; (b) Pellet viewed from above. Red arrow points towards the fracture; (c) Oriented templates in the fracture surface.

3.6 Piezoelectric characterization

The ceramic samples were ground to a thickness of 0.8 mm with 1200 grit SiC-paper, washed with 100 % ethanol in an ultrasound bath and dried. Silver electrodes were applied, dried and burnt in at 200°C over night.

Piezoelectric characterization was performed using an aixACCT aixPES system.

.

4 Results

4.1 Synthesis of $Bi_4Ti_3O_{12}$ templates

4.1.1 Particle size and aspect ratio

The average particle size and aspect ratio as functions of holding time and cooling rate are given in Table 4.1. Figure 4.1 presents the difference in particle size between samples heat treated at 1100°C with different holding times. The size and aspect ratio do not vary considerably.

Figure 4.2 shows the difference in particle size between two samples with different cooling rates after heat treatment. The sample with the lowest cooling rate exhibits the largest particles.

Table 4.1: Particle size of BiT templates with varying holding times and cooling rates.

Holding time at max. temp. [min]	Cooling rate [°C/hour]	Average diameter [μm]	Thickness [μm]	Aspect ratio
0	250	2.1±0.7	0.5±0.2	4.1
30	250	2.3±0.9	0.5±0.1	4.8
60	250	2.3±0.7	0.6±0.2	4.1
120	250	1.9±0.7	0.5±0.2	3.8
120	180	4.0±1.4	0.8±0.3	5.0

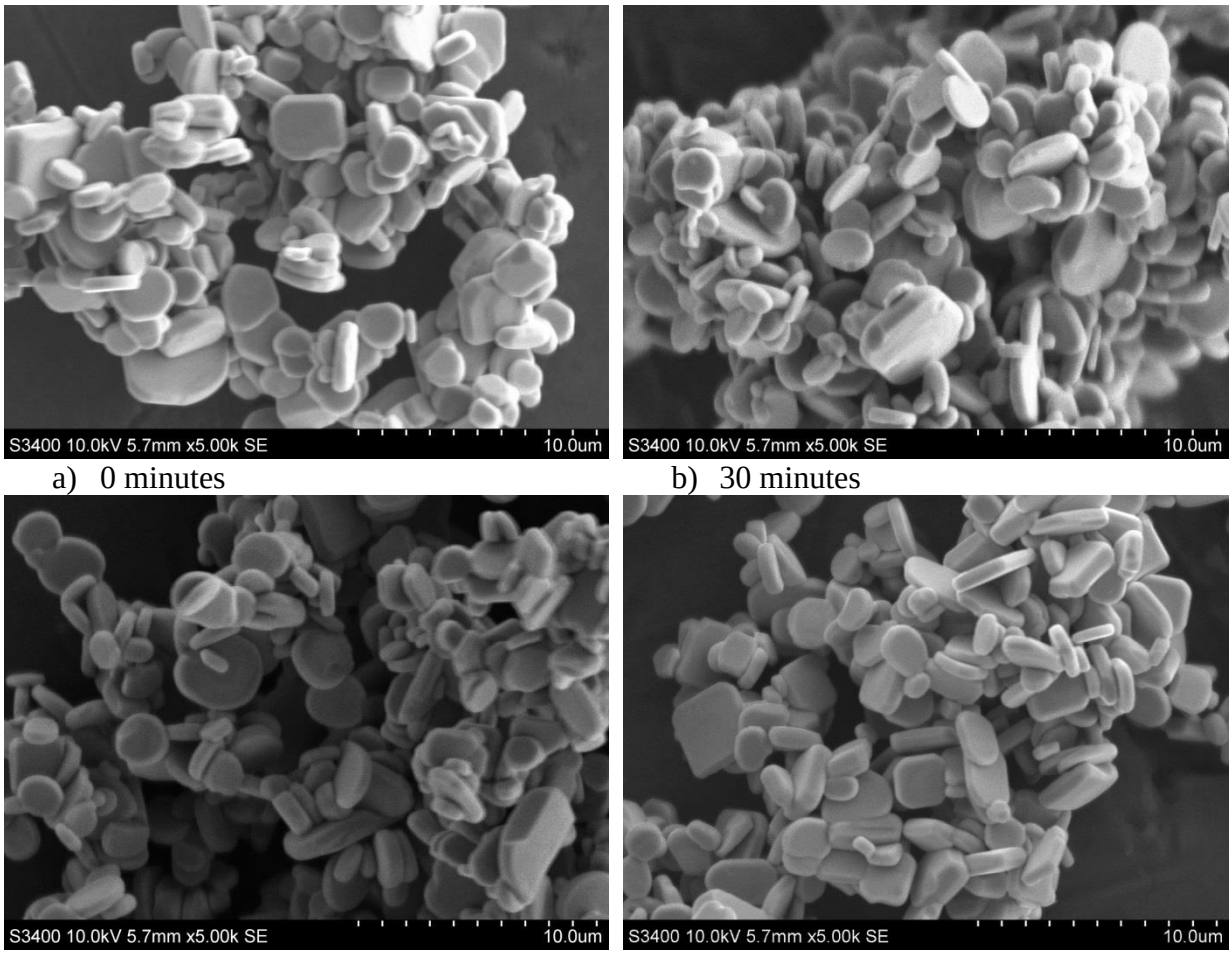

a) 0 minutes b) 30 minutes

c) 60 minutes d) 120 minutes

Figure 4.1: BiT templates synthesized at 1100 °C with different holding times, from 0 – 120 minutes. All samples have been cooled at a rate of 250 °C/h.

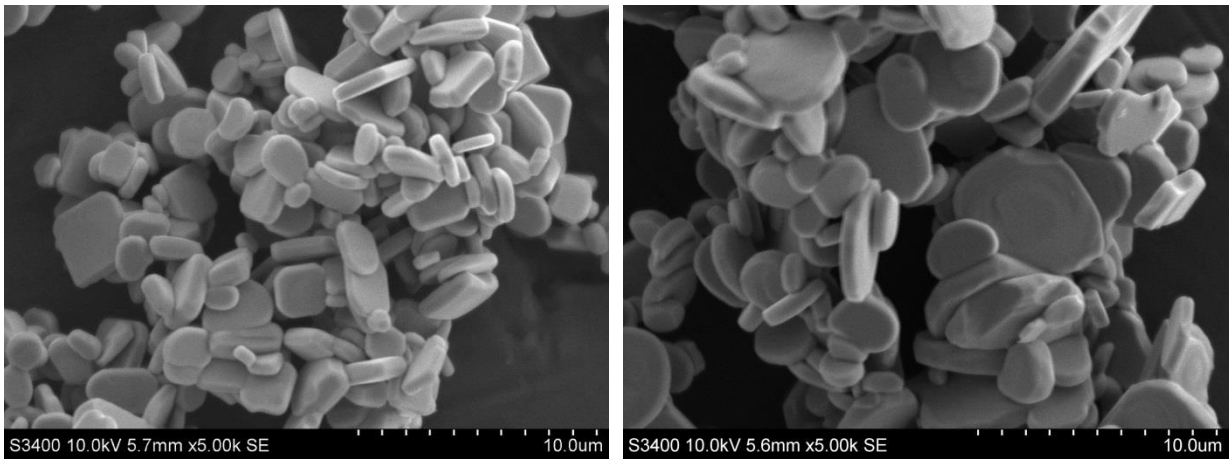

a) 250 °C/h cooling rate b) 180 °C/h cooling rate

Figure 4.2: BiT templates synthesized at 1100 °C for 2 hours with different cooling rates.

4.1.2 Phase purity and orientation

X-ray diffractograms of BiT templates are presented in Figure 4.3. Templates of the same sample, synthesized at 1100 °C for 2 hours with a cooling rate of 180 °C/h, have been prepared for X-ray diffraction (XRD) in two different ways, by conventional top filling and cast on a single crystal sample holder. The diffractograms display phase purity and preferential orientation of the templates, which is quantified by the Lotgering factor, calculated and reported in Table 4.2.

Table 4.2: Calculated Lotgering factors for a BiT sample prepared for XRD with conventional top filling and cast on a single crystal sample holder, using PDF card no. 00-035-0795 as reference.

Preparation	Lotgering factor, F [%]
Cast	38
Conventional	1

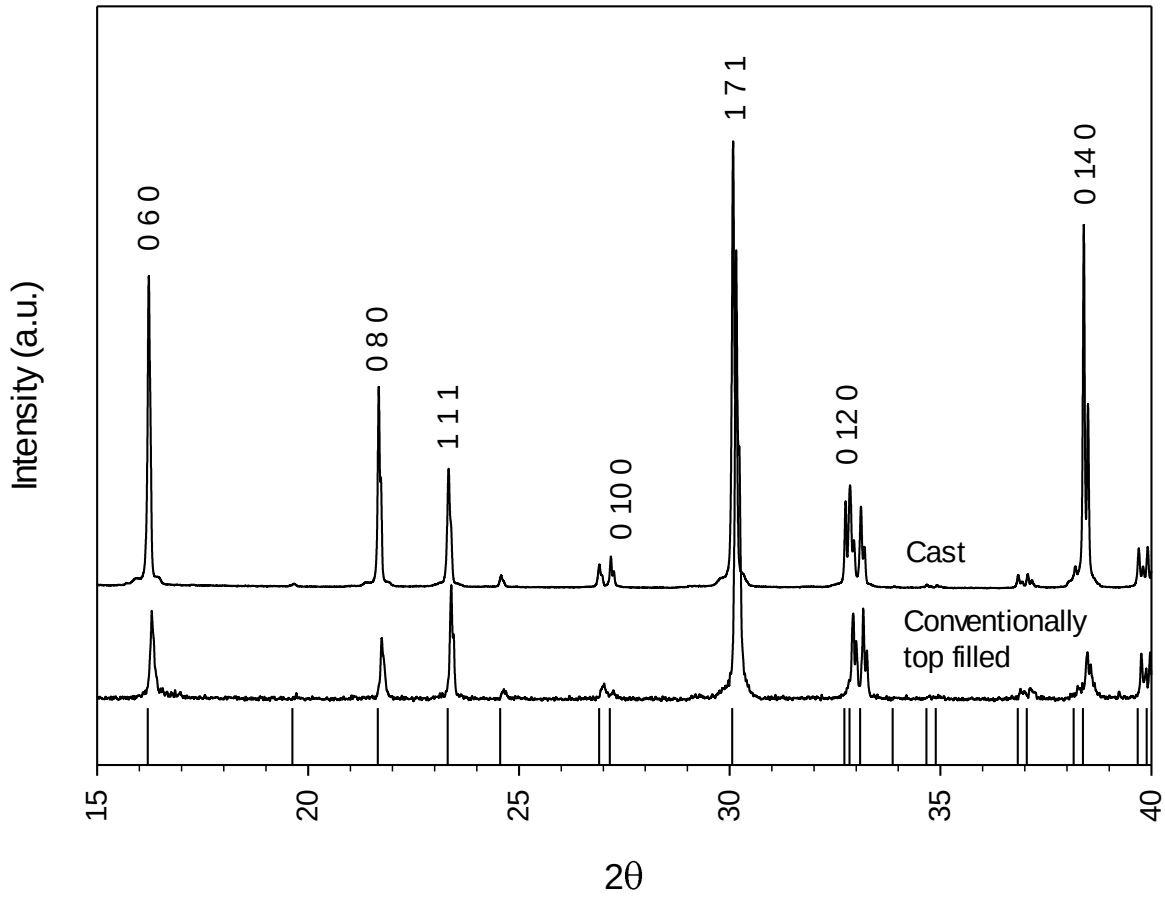

Figure 4.3: A comparison of BiT templates prepared for XRD scanning in two different ways, conventional top filling and cast on a single crystal sample holder. The samples have been normalized to the (1 7 1) diffraction line to make them comparable to each other. Selected diffraction lines are labeled. The vertical bars mark where the diffraction lines should be placed according to PDF card no. 00-035-0795.

4.2 Conversion of $Bi_4Ti_3O_{12}$ to $Bi_{0.5}K_{0.5}TiO_3$

Attempts to convert the BiT templates to BKT in molten salt were performed according to the following reaction:

$$Bi_4Ti_3O_{12} + 2K_2CO_3 + 5TiO_2 \rightarrow 8K_{0.5}Bi_{0.5}TiO_3 + 2CO_2 \qquad (4.1)$$

Figure 4.4 shows the morphology of a sample converted from BiT to BKT. The powder consists of large particle agglomerates as well as a number of "free" templates.

X-ray diffractograms of the samples compared to the diffractograms of BiT and BKT are shown in Figure 4.5. The samples are not phase pure.

Figure 4.6, 4.7 and 4.8 gives comparisons of the powder with changing parameters, showing overviews of the samples, the agglomerate constituents and the free templates, respectively. Figure 4.9 presents X-ray diffractograms of a sample where an attempt to separate the free templates from the powder has been made.

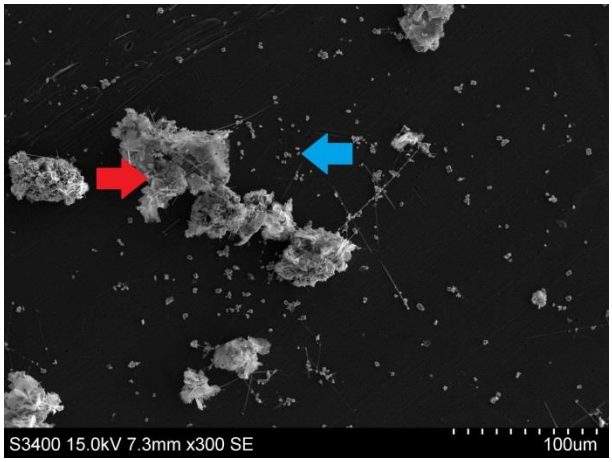

a) Overview of agglomerated particles and "free" templates. Agglomerates are marked with red arrow, "free" templates with blue arrow.

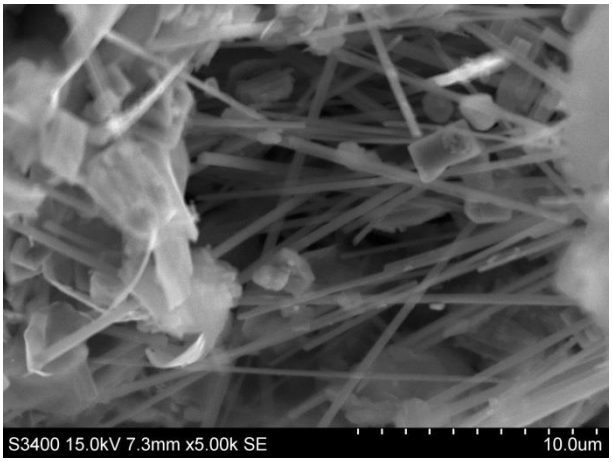

b) Magnification of agglomerated particles. Templates are entangled in whiskers.

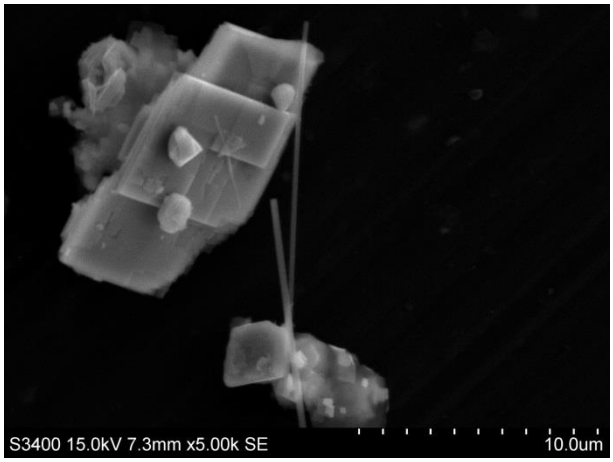

c) Magnification of free templates

Figure 4.4: Morphology of BiT converted to BKT for sample attempted converted at 950 °C for 4 hours with s/o ratio = 2. Note the different magnifications.

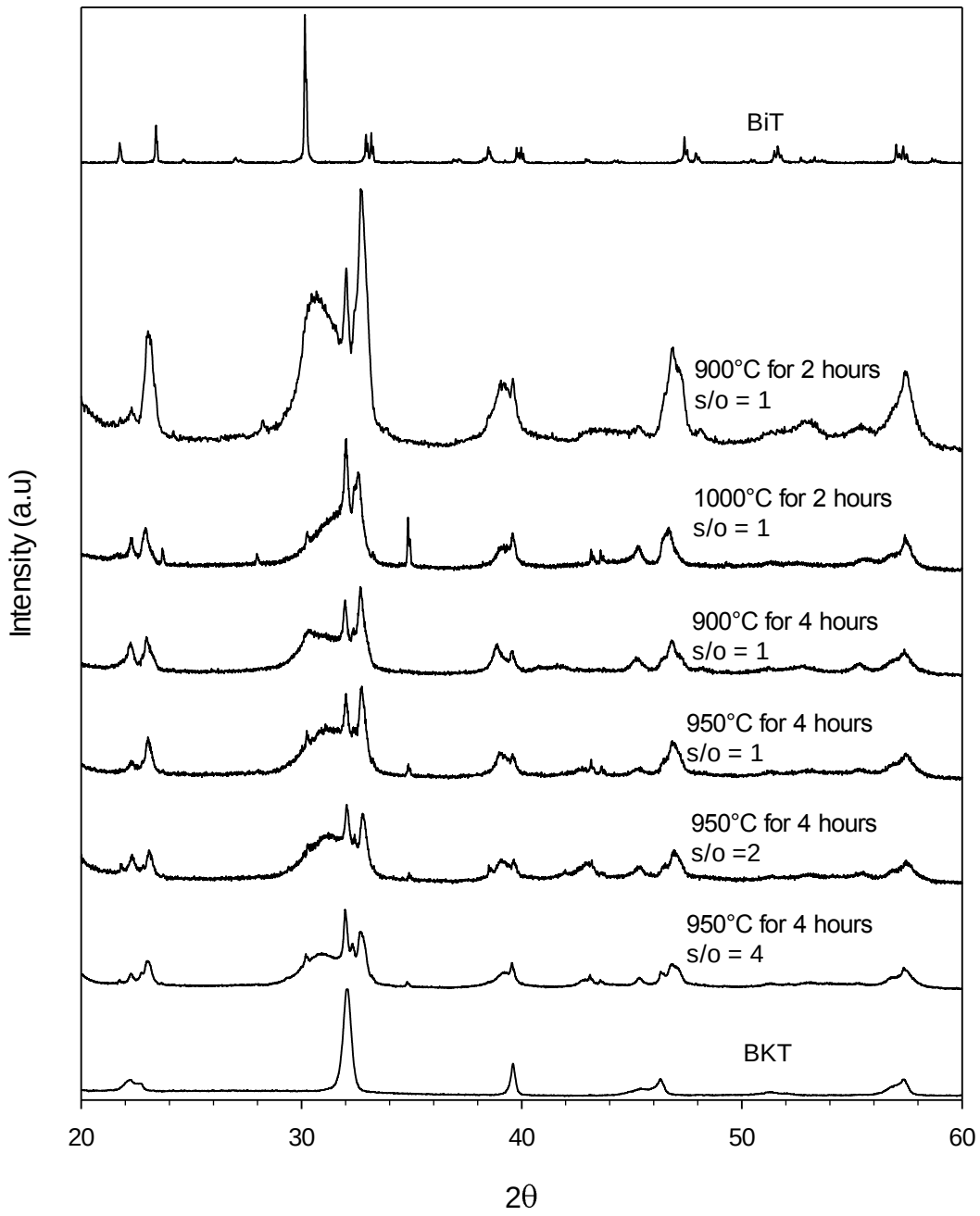

Figure 4.5: Diffractograms of BiT templates that have been attempted converted to BKT, compared with phase pure BiT and BKT. The samples have been synthesized at different temperatures with different holding times and varying salt to oxide ratio (s/o).

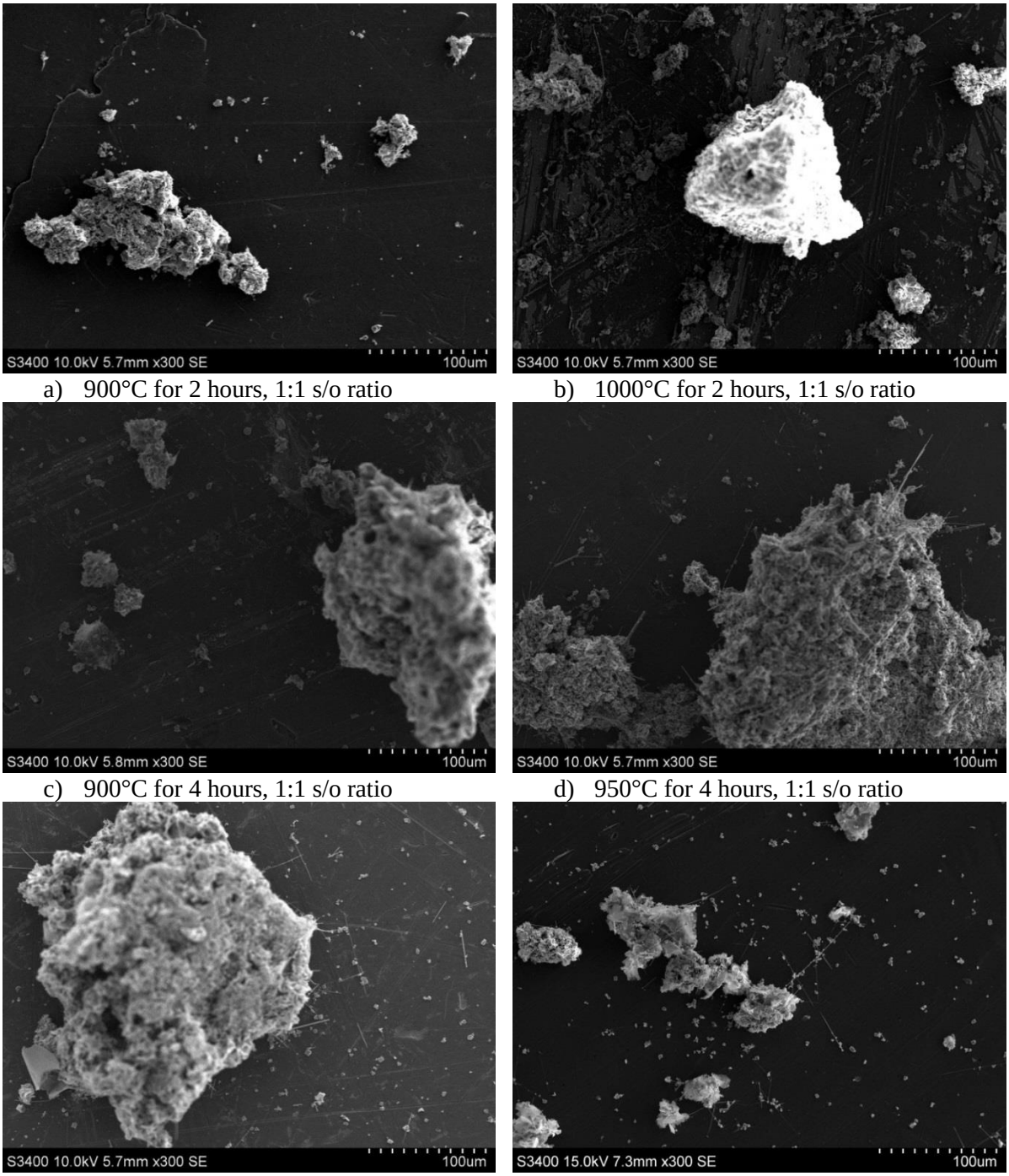

a) 900°C for 2 hours, 1:1 s/o ratio
b) 1000°C for 2 hours, 1:1 s/o ratio
c) 900°C for 4 hours, 1:1 s/o ratio
d) 950°C for 4 hours, 1:1 s/o ratio
e) 950°C for 4 hours, 2:1 s/o ratio
f) 950°C for 4 hours, 4:1 s/o ratio

Figure 4.6: Comparison of attempted converted samples at low magnification. The samples have been synthesized at varying temperatures, holding times and with different s/o ratio.

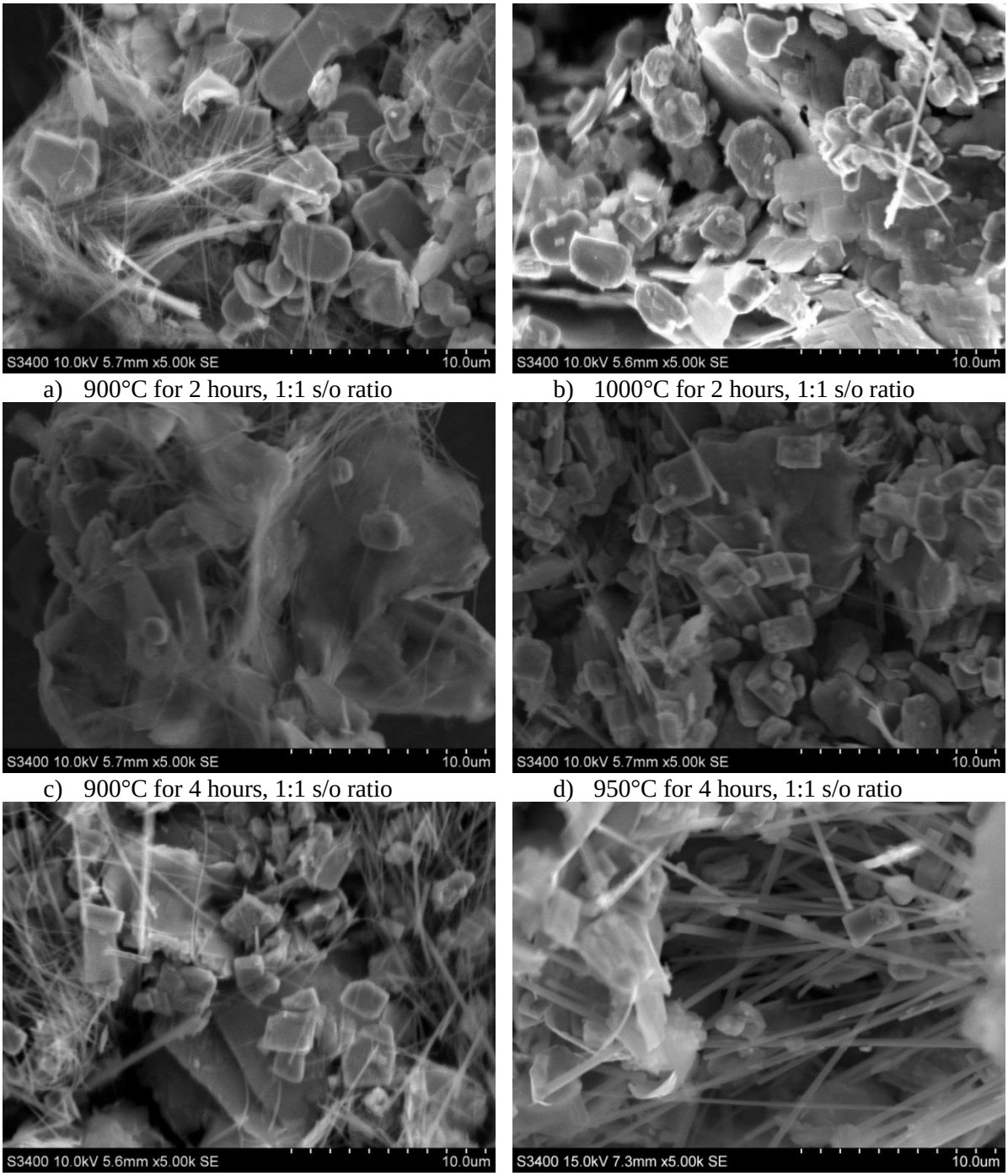

a) 900°C for 2 hours, 1:1 s/o ratio
b) 1000°C for 2 hours, 1:1 s/o ratio
c) 900°C for 4 hours, 1:1 s/o ratio
d) 950°C for 4 hours, 1:1 s/o ratio
e) 950°C for 4 hours, 2:1 s/o ratio
f) 950°C for 4 hours, 4:1 s/o ratio

Figure 4.7: Comparison of the agglomerate constituents of the attempted converted samples. The samples have been synthesized at varying temperatures, holding times and with different s/o ratio.

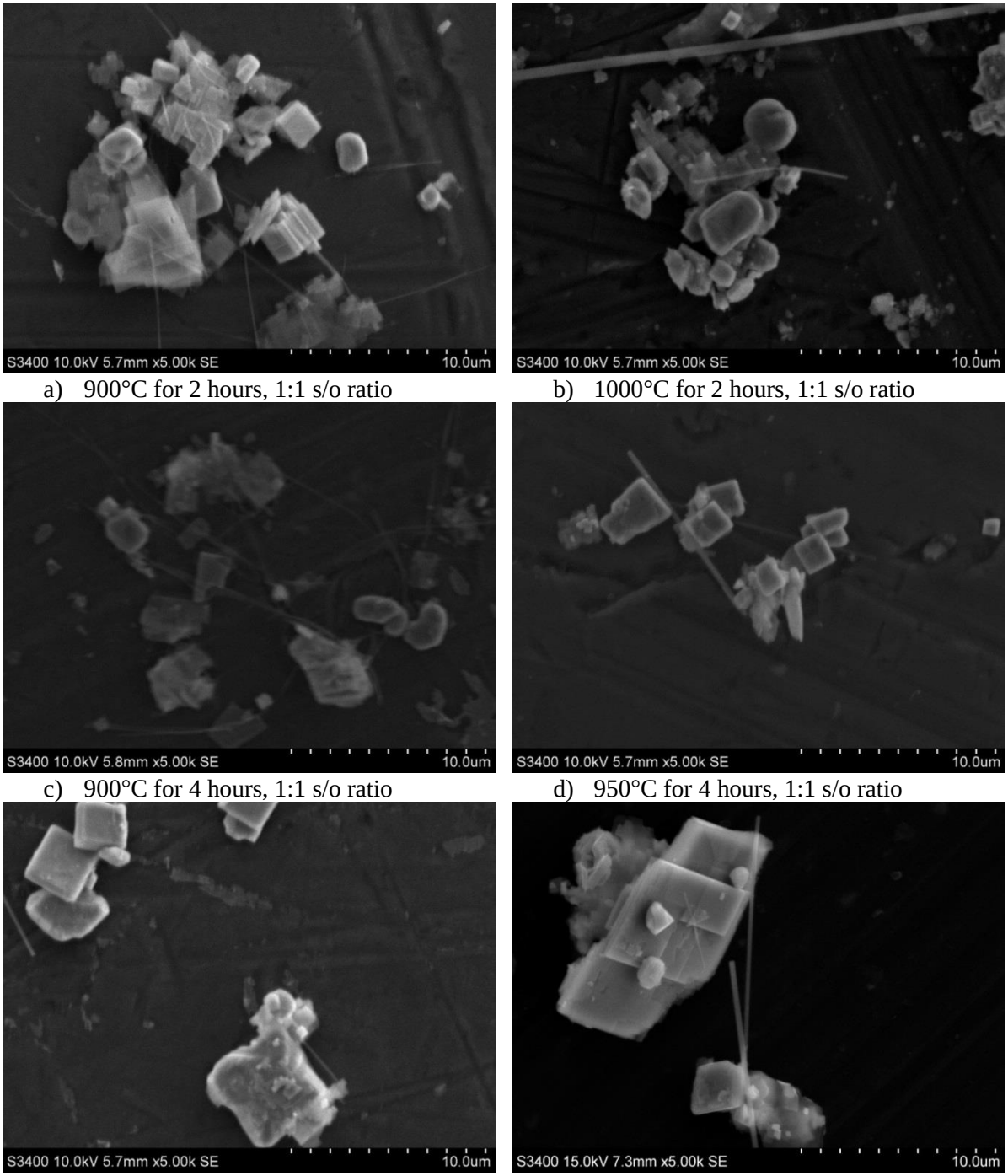

a) 900°C for 2 hours, 1:1 s/o ratio
b) 1000°C for 2 hours, 1:1 s/o ratio
c) 900°C for 4 hours, 1:1 s/o ratio
d) 950°C for 4 hours, 1:1 s/o ratio
e) 950°C for 4 hours, 2:1 s/o ratio
f) 950°C for 4 hours, 4:1 s/o ratio

Figure 4.8: Comparison of the free templates of the attempted converted samples. The samples have been synthesized at varying temperatures, holding times and with different s/o ratio.

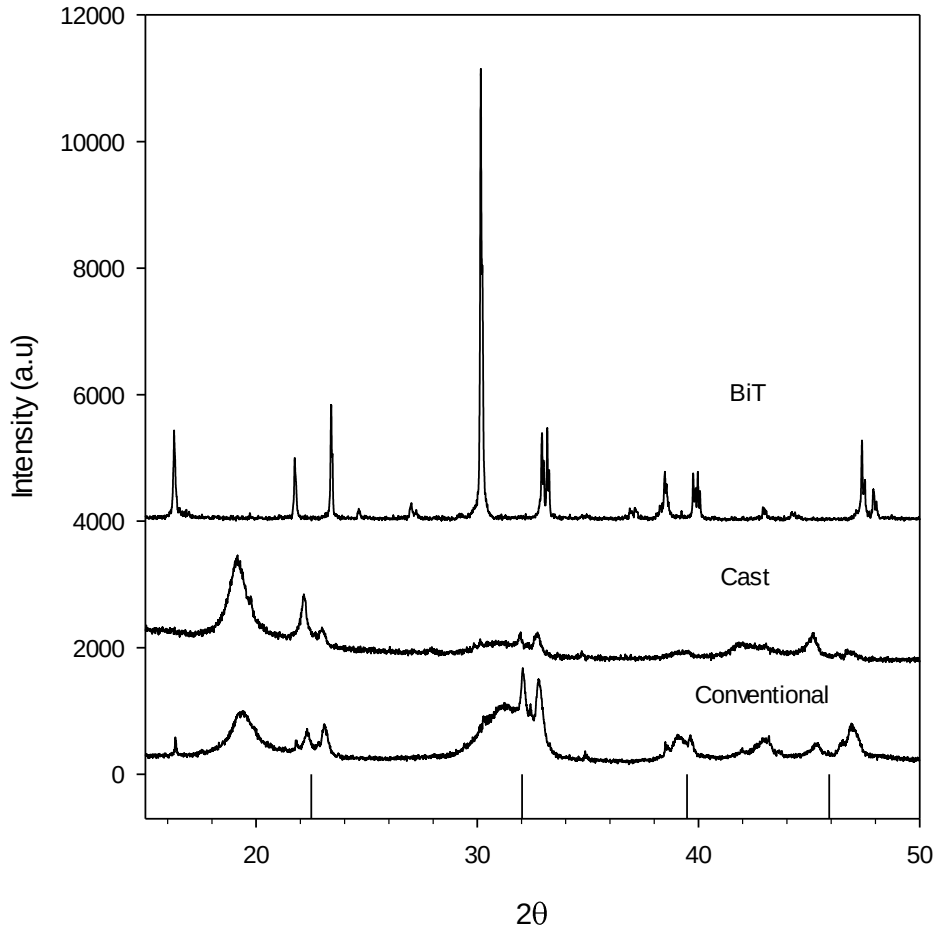

Figure 4.9: Comparison of an attempted converted sample prepared in two different ways: conventional top filling and cast on a single crystal sample holder. The vertical bars mark where the diffraction lines of BKT should be placed.

4.3 Production of ceramics

4.3.1 Production of matrix powder

The production of 0.75BKT-0.25BF powder is based on the method described by Morozov et al[8]. X-ray diffractograms of a small batch of powder (5 g) are presented in Figure 4.10, illustrating the phase purity after different calcination steps. Diffraction lines indicating secondary phases are present after the first calcination step at 800 °C, at ~23°, ~30° and ~33° 2θ. The intensity of these diffraction lines is lowered after remilling and a second calcination step at 860 °C. The diffraction lines have disappeared after sintering the powder to a ceramic pellet.

An X-ray diffractogram of a large (60 g) batch 0.75BKT-0.25BF powder is shown in Figure 4.11. No secondary phases are visible.

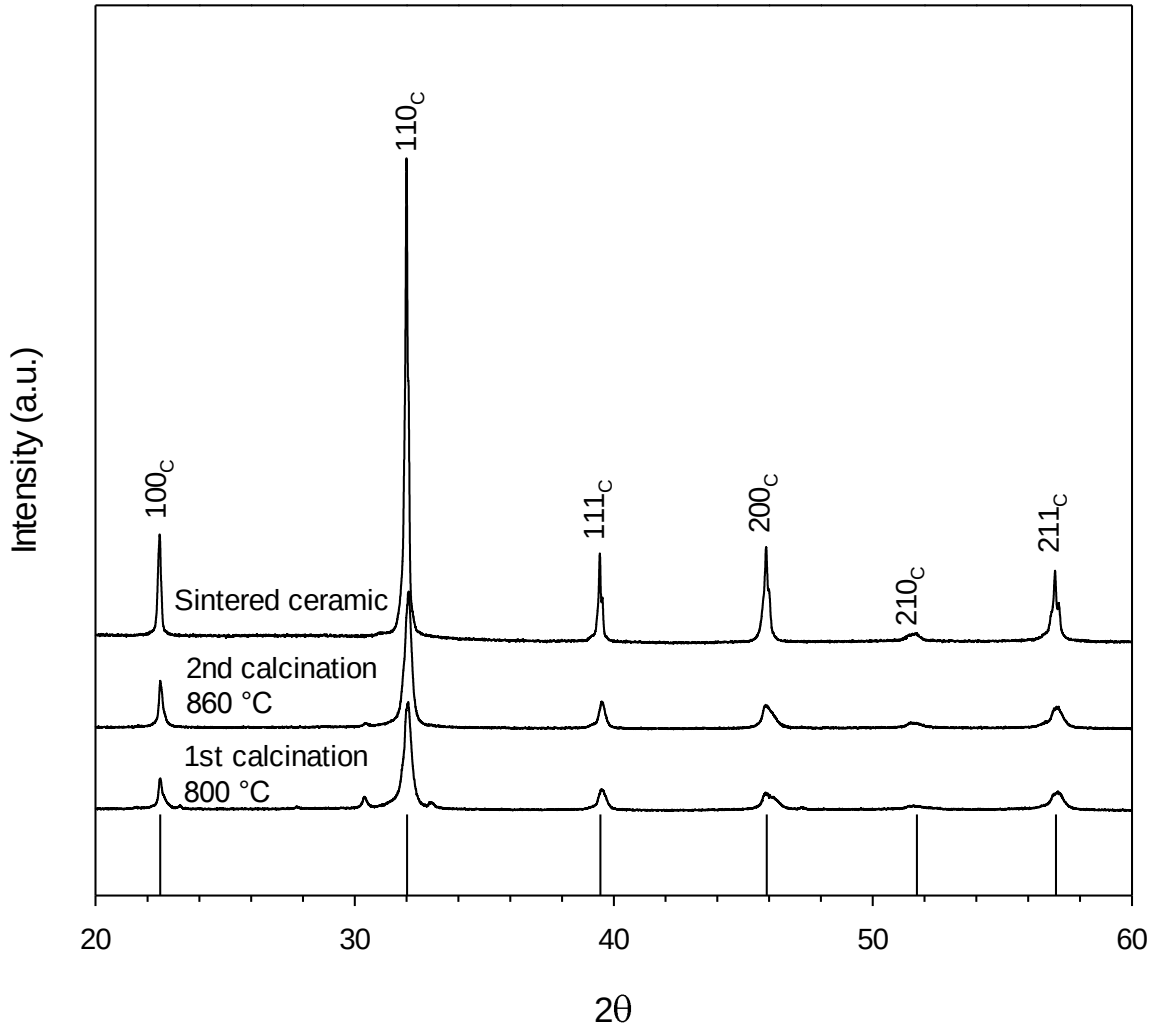

Figure 4.10: Diffractograms of a small batch of BKT-BF powder calcined twice at 800°C and 860°C and then sintered to a ceramic pellet. Diffraction lines are labeled with cubic indices.

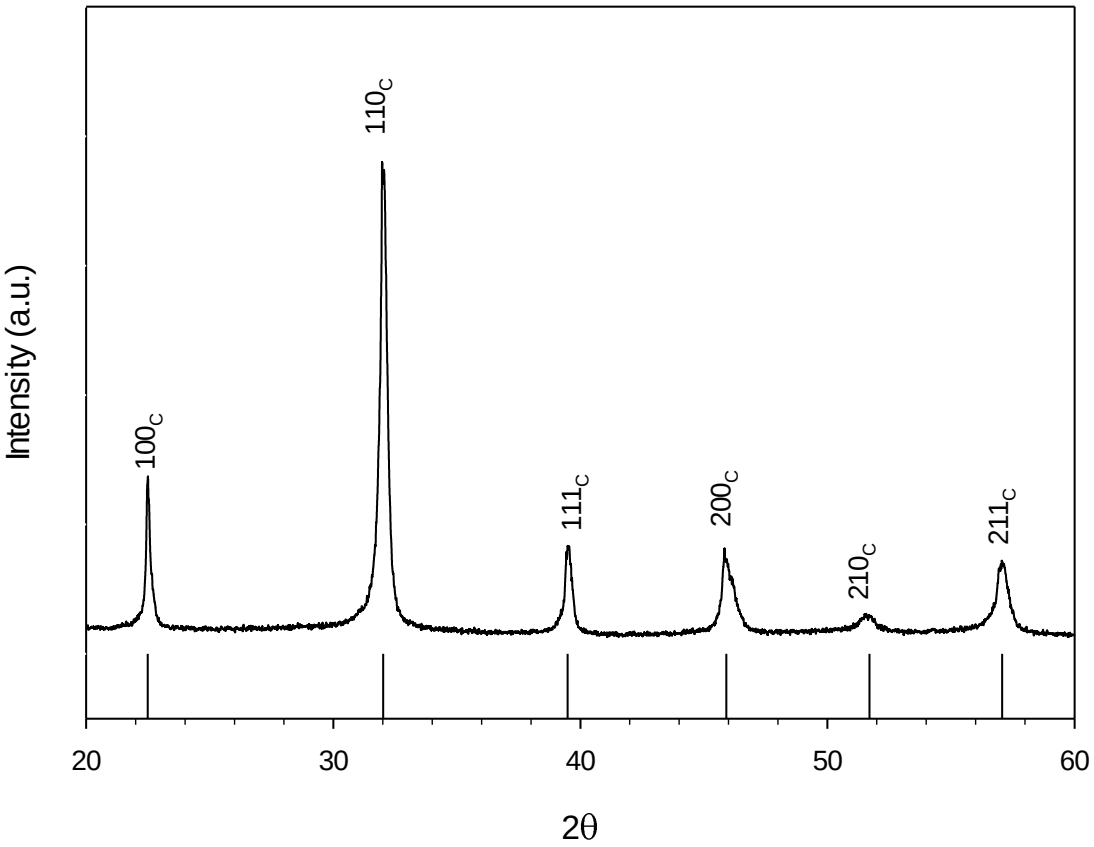

Figure 4.11: Diffractogram of a large batch calcined BKT-BF powder. Diffraction lines are given with cubic indices. The vertical bars mark the diffraction lines of perovskite structured BKT. The diffraction lines of the obtained diffractogram are slightly shifted from the bars due to different lattice parameters.

4.3.2 Production of ceramic samples

4.3.2.1 Untextured samples

The density and type of porosity of untextured BKT-BF ceramics are presented in Table 4.3.

Fracture surfaces of untextured samples sintered for 2 – 10 hours are shown in Figure 4.12, illustrating the increase in density and type of porosity. The samples sintered for 2 hours at 1080°C have much open porosity and are not finished sintering. The samples sintered at 1100°C have high densities and closed porosity. The sample sintered for 10 hours show substantial grain growth compared to the samples sintered for 2 hours.

X-ray diffractograms of the untextured samples are presented in Figure 4.13. The samples are mostly phase pure, though some impurities are present.

Table 4.3: Densities of pure matrix pellets with varying sintering temperature.

Sintering temperature [°C]	Sintering time [hours]	CIP	Density [%]	Open porosity [%]	Closed porosity [%]
1080	2	No	81	17.04	1.39
1080	2	Yes	86	13.27	1.77
1100	2	Yes	96	0.45	3.54
1085	10	Yes	95	0.36	4.24
1090	10	Yes	97	0	2.73
1095	10	Yes	97	0.39	2.77
1100	10	Yes	97	0.54	2.32

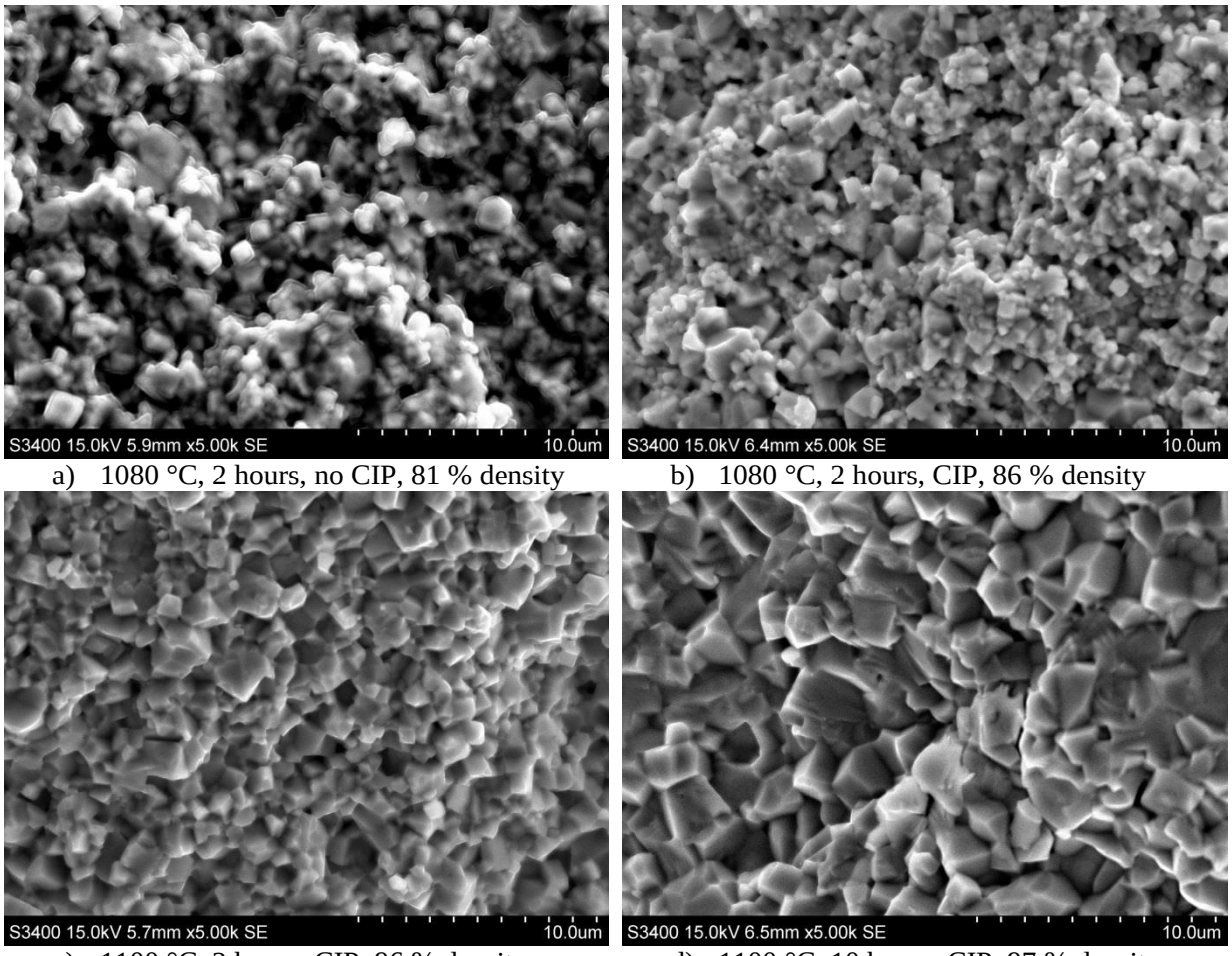

a) 1080 °C, 2 hours, no CIP, 81 % density
b) 1080 °C, 2 hours, CIP, 86 % density
c) 1100 °C, 2 hours, CIP, 96 % density
d) 1100 °C, 10 hours, CIP, 97 % density

Figure 4.12: Fracture surfaces of untextured BKT-BF samples sintered at different temperatures with different holding times at the sintering temperature.

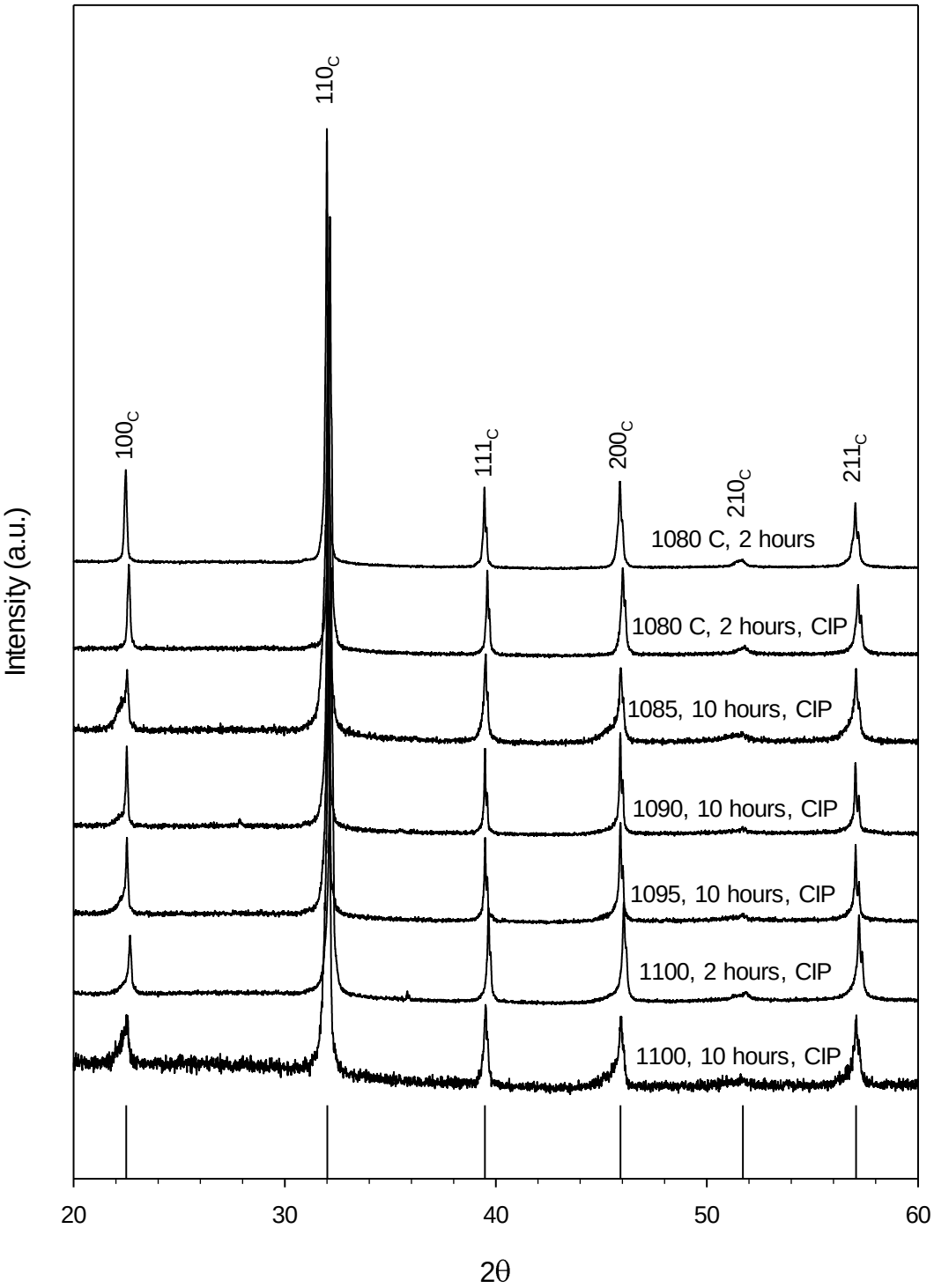

Figure 4.13: X-ray diffractograms of pure matrix pellets sintered at different temperatures with different holding times at the sintering temperature. Vertical bars represent diffraction lines of BKT.

4.3.2.3 Textured samples

Textured samples were produced by RTGG. BiT templates, K_2CO_3 and TiO_2 were added to a BKT-BF matrix and oriented with uniaxial pressing. The templates were converted in-situ to BKT as described in the following reaction:

$$Bi_4Ti_3O_{12} + 2K_2CO_3 + 5TiO_2 \rightarrow 8K_{0.5}Bi_{0.5}TiO_3 \qquad (4.2)$$

The difference in particle size between matrix powder and templates is illustrated in Figure 4.14. The size ratio has been calculated to 2.7.

X-ray diffractograms of textured samples sintered at different temperatures are shown in Figure 4.15. The diffractograms are mostly phase pure, but some impurities are present.

The densities and type of porosity of the textured samples are given in Table 4.4. Figure 4.16 shows the microstructure of a textured ceramic, which is characterized by large, closed pores surrounded by densely sintered grains.

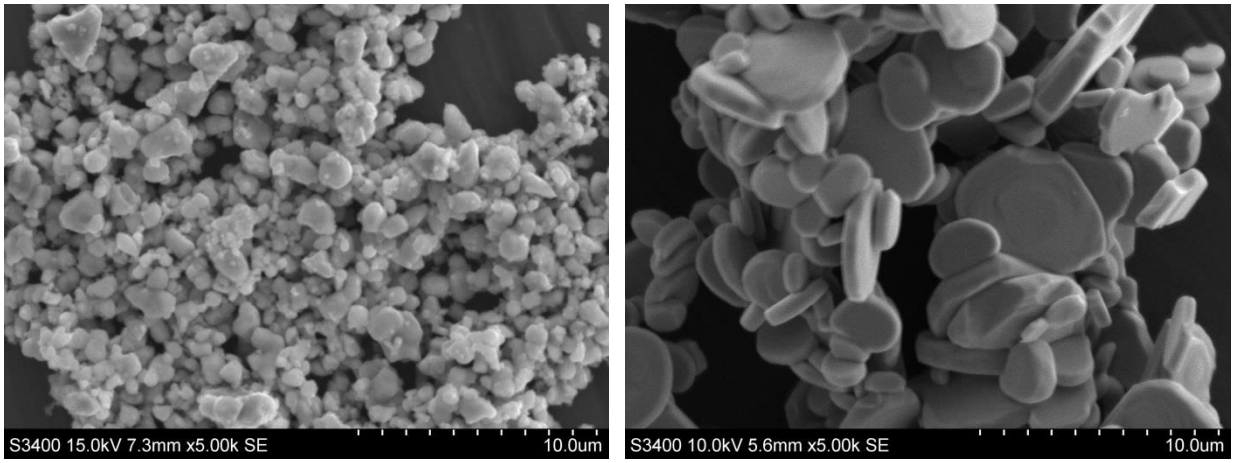

a) Matrix powder of 0.75BKT-0.25BF with average particle size 1.5 μm

b) BiT template particles with average particle size 4.0 μm

Figure 4.14: A comparison of the particle size of matrix powder and templates.

Table 4.4: Densities of textured ceramics with varying temperatures and amounts of BiT templates added to the matrix

Template fraction [%]	Temperature [°C]	Density [%]	Open porosity [%]	Closed porosity [%]
5	1080	92	0.72	6.83
10	1085	91	0.15	9.14
10	1090	92	0.20	7.73
10	1095	94	0.67	5.40
10	1100	93	0.87	5.69

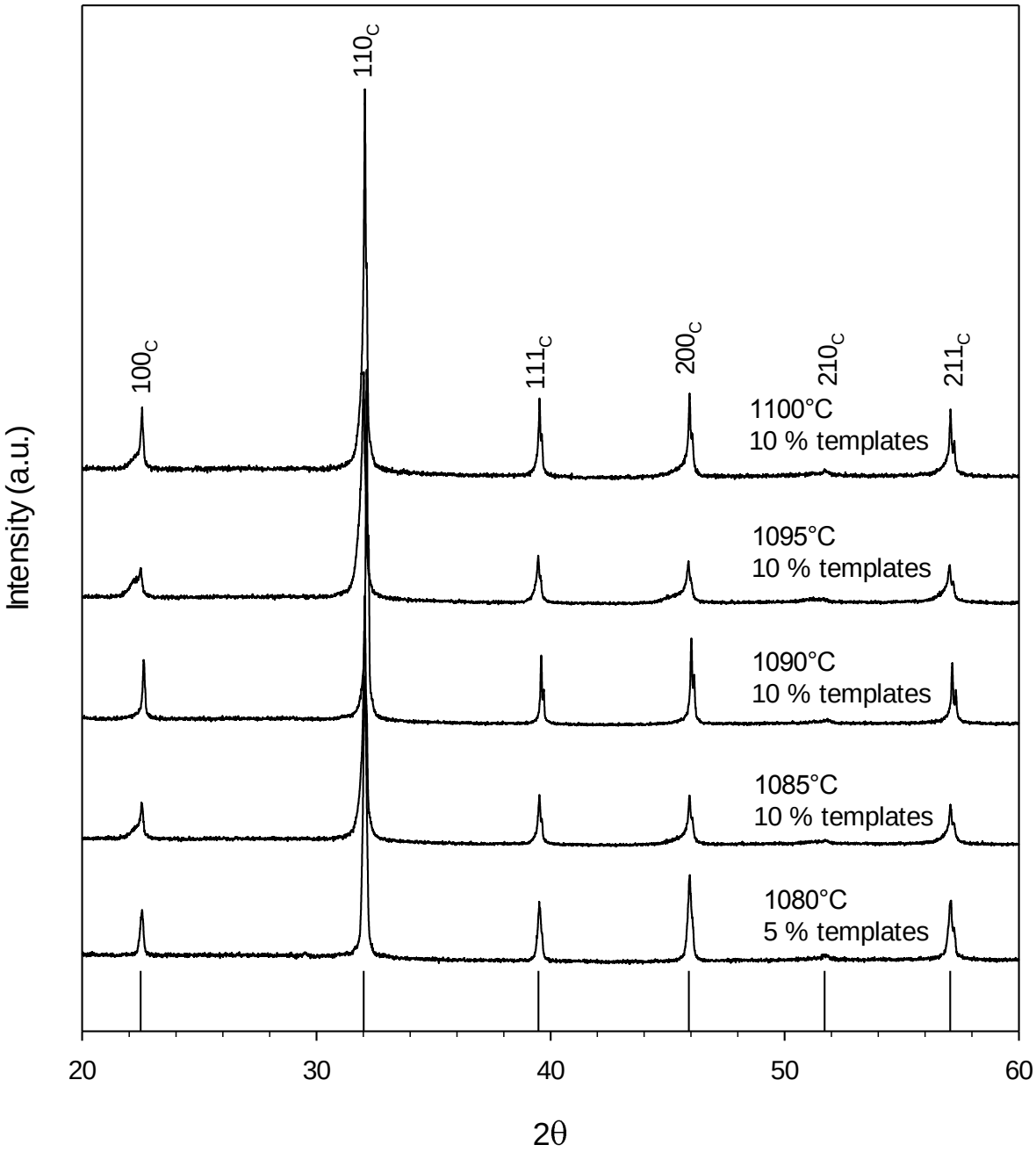

Figure 4.15: Diffractograms of textured pellets sintered at different temperatures with varying amounts of BiT templates added to the matrix. Vertical bars mark the diffraction lines of BKT.

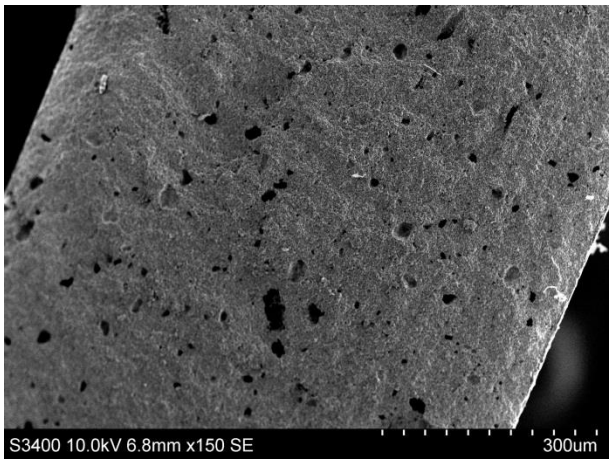

a) Overview of ceramic with large, closed pores.

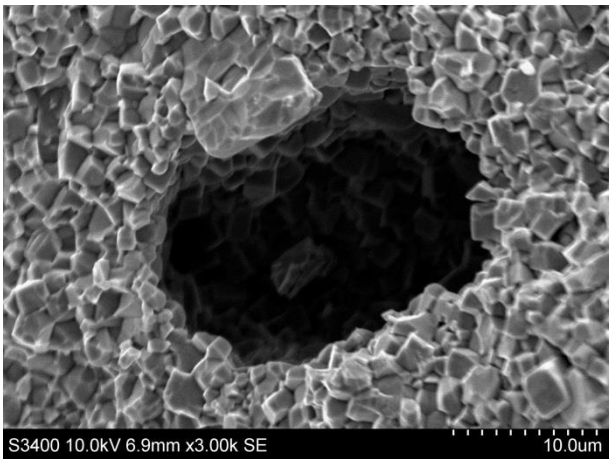

b) Closed pore.

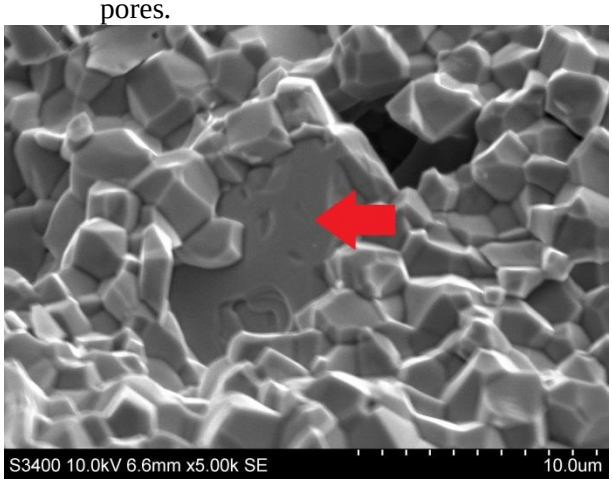

c) Template particle surrounded by equiaxed grains.

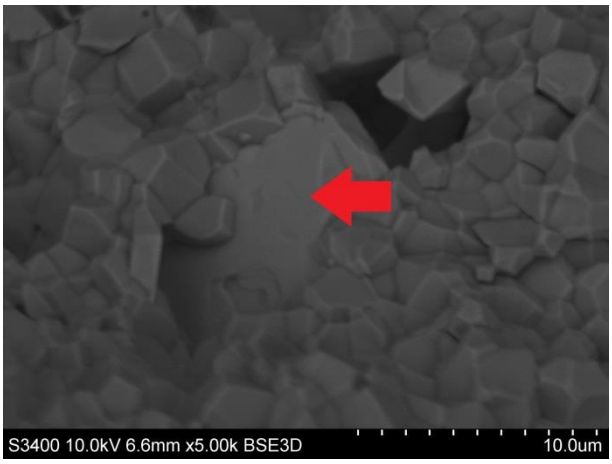

d) BSE-SEM micrograph of template particle surrounded by equiaxed grains.

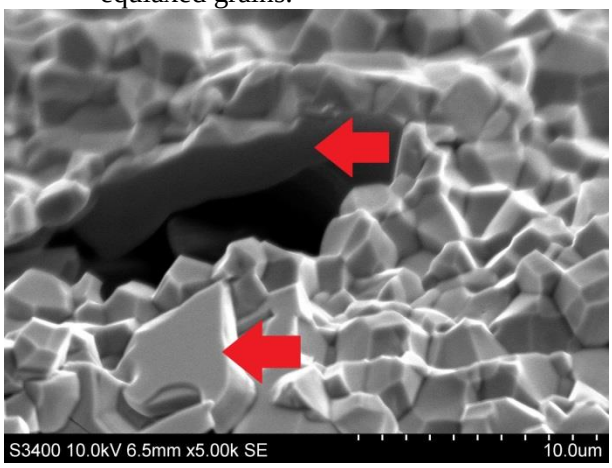

e) Template particles surrounded by equiaxed grains.

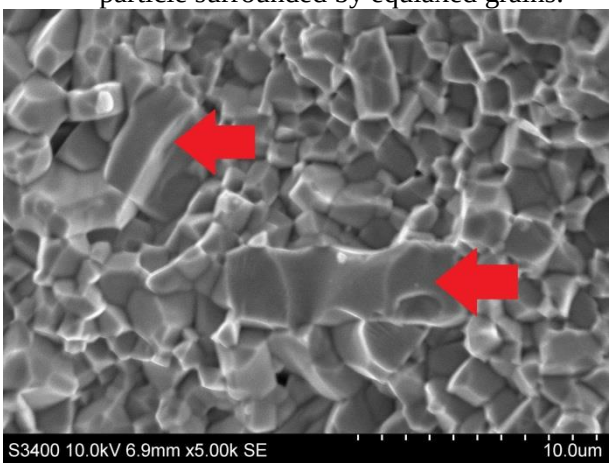

f) Template particles surrounded by equiaxed grains.

Figure 4.16: SEM and BSE-SEM micrographs showing the microstructure of a textured sample. Templates are marked with red arrows. Note the different magnifications.

4.3.3 Effect of texturing

4.3.3.1 Degree of texture

The calculated Lotgering factors of the textured samples are given in Table 4.5. The untextured ceramics sintered at the corresponding temperatures are used as references.

Table 4.5: Calculated Lotgering factor for textured samples.

Sintering temperature [°C]	Lotgering factor [%]
1080	3
1085	2
1090	0
1095	2
1100	3

4.3.3.2 Ferroelectric properties

Polarization as function of electric field for ceramic samples is given in Figure 4.17. The figure shows that all textured and untextured samples have high leakage current and are conductive.

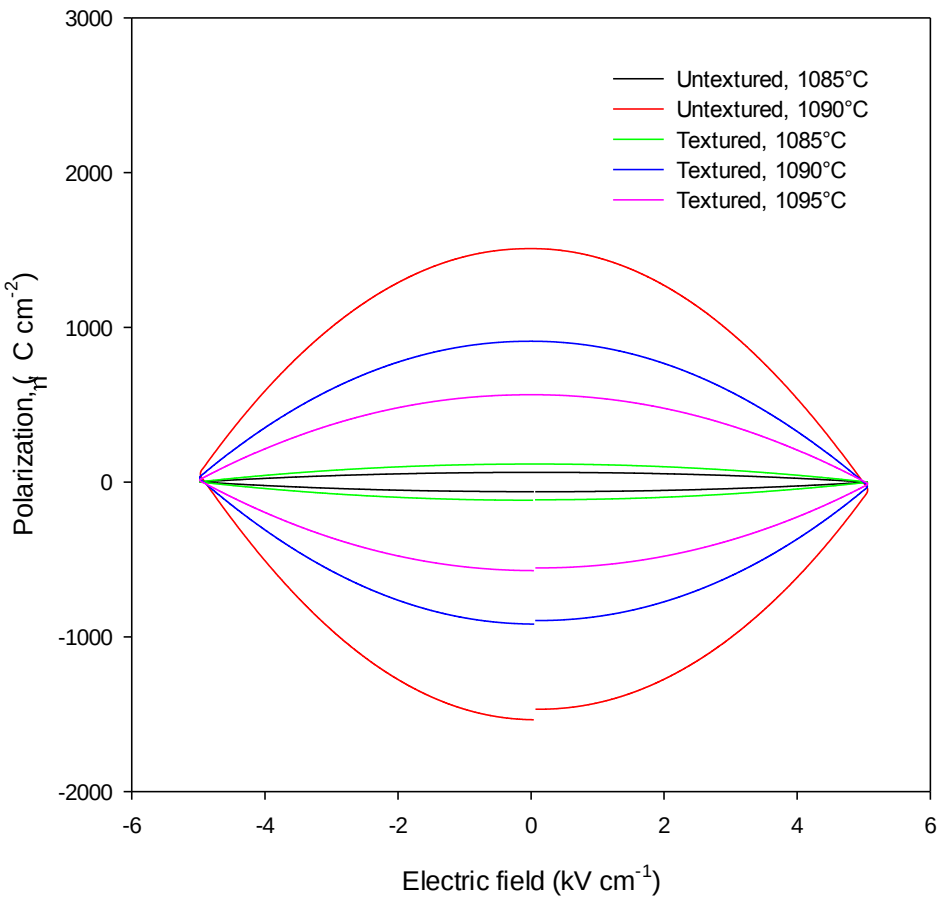

Figure 4.17: Polarization as function of electric field for textured and untextured samples.

5 Discussion

5.1 Synthesis of $Bi_4Ti_3O_{12}$ templates

The synthesis of bismuth titanate templates in this study is a continuation of the author's specialization project "Synthesis of bismuth titanate templates for tape casting of textured lead-free ferroelectric ceramics" [45], written as part of the Specialization Course TMT4500 the fall of 2012. Previous work has shown that higher s/o ratio does not increase the particle size and aspect ratio of the BiT templates. Longer heat treatment durations than 2 hours have been shown to decrease the aspect ratio. The particle size and aspect ratio have, on the other hand, been shown to be strongly dependent on the heat treatment temperature. Higher temperature results in larger particles and aspect ratios. As an extension of the previous synthesis optimization, the influence of shorter durations and cooling rates has been investigated.

Based on the decrease of the aspect ratio at long heat treatment durations, it was expected that the aspect ratios would increase with shorter holding times. This hypothesis was rejected, as shorter holding time during heat treatment did not produce templates with significantly higher aspect ratios. Instead the particle size seems relatively constant, as is seen in Figure 4.1 and Table 4.1. Slower cooling rates made a significant difference on the template particle size, which is evident from Figure 4.2. The particles in Figure 4.2a have a cooling rate of 250 °C/h and are generally smaller than the particles found in 4.2b, which have a cooling rate of 180 °C/h. All samples have a broad size distribution, which is explained by continuous nucleation and growth during cooling as the solubility of the oxides decreases as the salt flux cools. The size increase at slower cooling rates can thus be explained by precipitation and heterogeneous growth of oxides on the already existing particles rather than nucleation and growth of new ones.

The sample with highest aspect ratio (Table 4.1) was prepared for X-ray diffraction both on a conventional top filling sample holder and cast on a single crystal sample holder. The Lotgering factors of the two scans were then calculated. The difference in Lotgering factors between the two different sample preparations is as anticipated. The increase in the value of the Lotgering factor for the "single crystal diffractogram" is significant and can be explained by the plate shape of the templates. The templates will orient themselves with the flat side down giving preferential orientation when cast on a single crystal. When conventionally top filled, the templates are densely packed and randomly oriented. The particles therefore act as isotropic particles despite their individual anisotropy. The increased intensity of the diffraction lines corresponding to planes parallel to the (0 *l* 0)-direction demonstrates preferential growth in that particular direction, confirmed by the morphology seen in Figures 4.1 and 4.2.

5.2 Conversion of $Bi_4Ti_3O_{12}$ to $Bi_{0.5}K_{0.5}TiO_3$

5.2.1 Sample characteristics

The templates chosen for texturing must have a similar crystal structure with the desired phase, and a lattice mismatch of no more than 15 %. BKT would thus be the top candidate for TGG of BKT-BF. As described in chapter 2.5.2, the advantages of molten salt include increased diffusion rates and control of the morphology of the produced particles. MSS is frequently used for production of plate-shaped BiT, and topochemical conversion of BiT to BNT in molten salt has been performed successfully in several studies [41-43]. Both Na^+ and K^+ are alkali metals and behave similarly in several instances. It was hence anticipated that topochemical conversion in molten salt would be an appropriate method for converting BiT to BKT also.

Figure 4.5 show X-ray diffractograms of the attempted converted samples compared with pure BiT and BKT. The diffractograms of the produced samples are similar to neither BiT nor BKT, and clearly states that the samples are not phase pure. Diffraction lines placed at the same 2θ as the pure BKT diffraction lines point at the presence of some BKT in the samples. Generally, the diffraction lines of Aurivillius phases with different values of m lie close together, but are slightly shifted due to different lattice parameters. Thus, diffraction lines in the obtained diffractograms close or corresponding to the lines of BiT suggest that Aurivillius phases of unknown composition are present in the samples. It is therefore proposed that the conversion has occurred partially.

As seen in Figure 4.4, the converted samples consist of plate-shaped “free” templates and large agglomerates made up by plates entangled in long whiskers of unknown composition. An attempt to separate the free templates from the agglomerates was performed, described in chapter 3.5, with the aim of inspecting the composition of the free templates. Should the free templates be BKT, the conversion would be partially successful and it would be possible to separate the templates from the agglomerates for application in TGG. The result is found in Figure 4.9. The intensities of the diffraction lines have changed compared to Figure 4.5, indicating some preferential orientation. Otherwise the results are inconclusive.

The initial hypothesis was that the whiskers in the converted samples were due to a vapor-solid-liquid mechanism as a result of incomplete wetting of the oxides. The incomplete wetting might be due to a too low s/o ratio or the formation of gaseous CO_2 and volatile Bi-compounds during the heat treatment. However, increasing the amount of KCl did not eliminate the whisker production. This will be further discussed in chapter 5.2.2. Rørvik et al. [46] produced sodium titanate nanowires during production of perovskite $PbTiO_3$ and $BaTiO_3$ nanorods in molten NaCl. They demonstrated that the stoichiometry of the desired nanorods was hard to control due to formation and volatility of $BaCl_2$ and $PbCl_2$. It was suggested that the presence of these volatile species promotes deviations in the initial Pb/Ti-ratio when the amount of cation precursor relative to the salt is small, with formation of nanowires as a result. The produced nanowires were not detectable by XRD, only with TEM and SEM. Interestingly the nanowires were not formed in the absence of salt, but the fraction of

nanowires decreased with increasing amounts of salt. There are many similarities between the work performed by Rørvik et al. and this study. In this work KCl was applied as molten salt flux instead of NaCl, and the desired product was $Bi_{0.5}K_{0.5}TiO_3$. Potassium is in the same elemental group as sodium. Bi_2O_3 may react with salt and produces $BiCl_3$, which is a very volatile species. Hence, it is proposed that the observed whiskers in this study may be potassium titanate whiskers, formed through a similar mechanism as in the study performed by Rørvik et al. The batches of produced powder were small (5 g), which makes the system vulnerable to small deviations in stoichiometry and inhomogeneous mixing. When $BiCl_3$ evaporates the ratio between the precursors is no longer stoichiometric, which combined with local variations in mixture homogeneity may have caused the formation of the whiskers.

5.2.2 Parameter optimization

In general, increasing the reaction temperature increases the diffusion rate and thus the reaction rate. Consequently, it was expected that increasing the temperature of the conversion from BiT to BKT would improve the reaction's degree of completion. However, Figure 4.5 demonstrates that the X-ray diffractograms of conversions do not show increased similarity to the diffractogram of BKT with increasing temperature. On the contrary, an extra diffraction line shows up at ~32° 2θ. The intensity of this diffraction line increases with increasing temperature, so increasing the temperature is disadvantageous. No changes in morphology are detectable with increasing temperature, as seen in Figures 4.6, 4.7 and 4.8.

The motivation for increasing the holding time at the conversion temperature was the possibility that the conversion was kinetically hindered. However, no apparent differences occur in the X-ray diffractograms in Figure 4.5 with increasing holding time. The morphology of the sample powder (Figures 4.6, 4.7 and 4.8) did not change noticeably. It is possible that the increase in holding time is too low to make a significant difference, and that doubling the holding times another time would improve the reaction.

An increased amount of KCl means more liquid at the conversion temperature. As the obtained whiskers were believed to be a result of inadequate wetting of the oxide surfaces, the s/o ratio was doubled twice to improve this. The only detectable change is an increase in the particle size of the free templates, found in Figure 4.8e and f, but the whiskers are still present in substantial amounts, similar to what was found by Rørvik et al.

None of the parameter alterations executed in this work improved the conversion to BKT. Based on the obtained results molten salt synthesis is an unsuitable method for conversion of BiT to BKT.

5.3 Characteristics of ceramic samples

5.3.1 Production of the matrix powder

The desired product phase has a cubic-like perovskite structure, suggested by the X-ray diffractograms in Figure 4.10. The diffractogram obtained after the first calcination step at 800°C of the small powder batch in Figure 4.10 indicates that the reaction was not completed. The diffractogram exhibits extra diffraction lines, i.e. at ~23°, ~30° and ~33° 2θ. The intensities of these diffraction lines are lowered after the second calcination step at 860°C and vanish after sintering the powder to a ceramic pellet. The X-ray diffractogram of the large powder batch in Figure 4.11 shows that the powder is phase pure and a second calcination step was not necessary. The small batch was mixed by hand with mortar and pestle, while the large batch was mixed by ball milling. It is therefore suggested that the incomplete reactions of the small batch are due to inhomogeneous mixing. Small batches are more sensitive to stoichiometry errors arising during processing, from evaporation of volatile species or long diffusion distance, while large batches are less sensitive to such flaws. The phase purity of the sintered pellet suggests that a second calcination step is unnecessary regardless of the size of the powder batch.

5.3.2 Density and microstructure

The untextured ceramics sintered for 2 hours represents an attempt to reproduce the ceramics made by Morozov et al. [8]. Difficulties achieving high densities, >95 % [7], were encountered. The density of the ceramics increased substantially when using CIP, but the density did not reach sufficient values. Table 4.3 and Figure 4.12a and b clearly show that a sintering temperature of 1080 °C was not sufficient to complete sintering as the samples are characterized by high percentages of open porosity. A dramatic increase in density is achieved upon increasing the sintering temperature to 1100 °C, producing ceramics with high density. To produce samples with equal thermal history to the textured samples the sintering temperature was increased from 2 to 10 hours. All the 10 hour samples are dense. Longer sintering times are therefore beneficial with respect to density, though considerable grain growth is observed (Figure 4.12d).

As given in Table 4.4, the textured samples achieved lower densities than the untextured samples, 91 – 94 %. The microstructures are characterized by large, closed pores surrounded by densely sintered grains, as seen in Figure 4.16a and b. The main particle size of the densely sintered grains in the textured samples is comparable to the particle size of the untextured samples with the same thermal history (Figures 4.12d and 4.16c). The pores observed in the textured samples are large, with a diameter of 10 μm and higher. These voids could be caused by large grains that have been pulled out during the fracture. As no such grains are observed elsewhere on the fracture surfaces, this is unlikely. The conversion of BiT to BKT produces CO_2 during sintering. If this CO_2 gas is trapped in the structure during sintering, forming gas bubbles, it may have caused the large voids observed in the structure. A more likely explanation is agglomerated precursors, i.e. K_2CO_3. The precursors were measured and mixed in small quanta (1.6 g), crushed and mixed by mortar and pestle. These agglomerates might have caused non-uniform packing during the uniaxial pressing and have left voids where the

agglomerates were placed before decomposition and diffusion. To avoid large agglomerates in the future, mixing and crushing large batches with ball milling before addition of template particles may be an alternative, though controlling the stoichiometry before sintering will be harder.

The textured samples contain 5 – 10 wt% template particles. These particles are visible in the microstructure, surrounded by equiaxed grains. Figure 4.16c-f show plate shaped particles in the microstructure which are considerably larger than the surrounding particles. The micrographs of the fracture surfaces are taken normal to the direction of uniaxial pressing/orientation, as illustrated in Figure 3.2. If the templates were sufficiently oriented, the thin edge of the particles would be visible in the microstructure. However, this is not the case. Instead the templates are randomly oriented in the microstructure.

5.3.3 Phase purity

The X-ray diffractograms in Figure 4.13 show that the untextured samples are mostly phase pure. All samples have been produced from the same batch of matrix powder. Some of the samples exhibit extra diffraction lines, representing unidentified secondary phases. However, the secondary phases do not occur systematically, as the diffraction lines occurring in the different samples have are placed at various 2θ values.

The X-ray diffractograms of the textured samples (Figure 4.15) show that the samples are mostly phase pure. Small signs of secondary phases occur in some samples, but the intensities of these are low. The phase purity is supported by the BSE-SEM micrograph in Figure 4.16d, which does not show variations in color. The phase purity of the samples demonstrates that the in-situ conversion of the Aurivillius structured templates to perovskite structure was successful. The BSE-SEM micrograph shows that all the particles are of the same composition, as there are no apparent color variations. This means that the BiT templates are not converted to BKT, but to BKT-BF. As only reactants needed for conversion to BKT was added to the matrix, it is suggested that the composition of the structure has been displaced towards BKT. Calculations give a new composition of ~0.78BKT-0.22BF.

5.3.4 Degree of texture

Uniaxial pressing was chosen as technique of orienting the templates. Commonly applied techniques for this purpose are extrusion or tape casting. These methods are effective, but laborious and time consuming. Considerable time would be saved if the templates could be oriented by uniaxial pressing only.

The degree of texture is quantified as the Lotgering factor given in Table 4.5, and varies from 0 – 3 %. These values are low [7] and indicates lack of texture. This is supported by the SEM micrographs in Figure 4.16c-f. The micrographs of the fracture surfaces are taken normal to the uniaxial pressing direction, as illustrated in Figure 3.2a. If the templates were oriented by the pressing, they would be oriented as shown in Figure 3.2c. Instead, the templates are visible as randomly oriented plates in the matrix. It is possible that high uniaxial pressures would orient the templates in the matrix more efficiently. However, higher pressure means

higher likelihood of introducing pressing defects in the green body, hindering the ceramic to sinter to high densities.

The size difference between the templates and the matrix powder is calculated to 2.7 (Figure 4.14), which is thermodynamically high enough to sustain Ostwald ripening. Boundary motion is restrained by pores, so significant grain growth cannot occur until >95% density has been achieved. Once this density is reached, the template growth is rapid [7]. The textured samples contain several large pores, and the densities vary between 91 – 94 % (Table 4.4), which may be a partial explanation to the lack of texture as the large pores hinder exaggerated grain growth of templates in their vicinity. The observed templates (Figure 4.16) are large compared to the surrounding matrix, indicating that exaggerated grain growth has happened to a certain extent in locally dense areas of the ceramic. There is a possibility that sintering times exceeding 10 hours would have given the templates time to grow more at the expense of the matrix particles. However, the random orientation of the templates counteracts the benefits arising from the growth of the templates. Based on the observed lack of texture it is proposed that uniaxial pressing is not sufficient to orient the template.

5.3.5 Ferroelectric behavior

The polarization of a ferroelectric material with an externally applied electric field is characterized by a hysteresis curve as shown in Figure 2.5. The curves exhibited by the ceramics in this work (Figure 4.17) are shaped differently. They are elliptical, showing that there is much leakage current in the samples, making the ceramics conductive. Hence, the produced samples are not ferroelectric, despite the system being a known ferroelectric.

The textured samples, depicted in Figure 4.16, have large, closed pores. Such pores may be a source of leakage current, which would be a plausible explanation of the conductivity of the textured samples. However, it is important to note that both textured and untextured ceramics are conductive. One can thus conclude that the error is systematic, and must concern all the samples.

The X-ray diffractograms (Figure 4.13 and 4.15) seems phase pure at first glance, which is supported by the SEM and BSE-SEM micrographs (Figure 4.12 and 4.16). No secondary phases are visible on the fracture surfaces. However, as pointed out in chapter 5.4.3, the diffractograms in Figures 4.13 and 4.15 exhibit small signs of secondary phases. Despite occurring in only a selection of the samples, it is possible that the impurities are present in all the samples without being detected. As described in chapter 3.5, a slit of 0.2 mm was used for recording the diffractograms. The intensities of the secondary phase diffraction lines are so low that it is possible that the information has not been recorded during scanning of the samples not exhibiting such diffraction lines. One can imagine that such secondary phases are present in amounts large enough to cause conductivity without being enough to be detected by X-ray diffraction. The impurities are thus proposed as a possible explanation of the conductivity exhibited by the produced ceramics. They may have been obtained during processing, i.e. from insufficient cleaning of the pressing tools.

5.4 Summary

BiT is a suitable material both for direct application as templates in TGG and as a precursor for other templates. As the ratio between the template and matrix particles influences the rate of template growth during sintering, it is important to produce as large particles with as high aspect ratios as possible. The thermodynamic limit is a ratio of 1.5, but higher values are preferred due to kinetic considerations. The size ratio between the average diameter of the pure BiT particles produced in this study and the BKT-BF matrix particles was calculated to 2.7. Higher values than 2.7 would be preferable, both because of the kinetics of the template growth, but also because templates with high aspect ratios are easier to orient in the matrix prior to sintering. On the other hand, the templates synthesized in this work may be more suitable to the chosen orienting method as the thickness of the particles make them sturdy enough to endure uniaxial pressing.

The initial plan was to texture the BKT-BF through TGG. TGG is a simpler process than RTGG, as the template conversion is already finished. RTGG involves diffusion of reactant particles, which, depending on the quality of the mixture, may be difficult due to long distances between the reactants. However, the conversion of the BiT templates to BKT in molten salt was unsuccessful. RTGG was therefore performed as an alternative method and worked well with regards to in-situ conversion of the templates. As pointed out in chapter 5.3.3, the textured samples are phase pure with the same phase in both templates and matrix powder. This means that the whole ceramic is of the same composition, BKT-BF. K_2CO_3 and TiO_2 were added to the matrix to convert the BiT templates to BKT, but no Fe_2O_3 was added. The resulting structure is thus not 0.75BKT-0.25BF, but slightly shifted away from the MPB towards BKT. Calculations give a new composition of 0.78BKT-0.22BF.

An increase in the degree of texture would be visible through high Lotgering factors, be visually confirmable by the microstructure, an increase of the piezoelectric coefficient would be measured and a strong anisotropy in the measured ferroelectric hysteresis loop would be found. The ceramics produced in this study are conductive, making comparison of electromechanical properties between textured and untextured samples impossible. But even if the samples were ferroelectric, the untextured and textured samples would still not be comparable due to their different compositions. If the ceramics were of the same composition and not conductive, it is possible that increased properties would not be exhibited due to the measured lack of texture.

Consider the case of a situation where the conversion of BiT to BKT through MSS was successful and the templates suitable for texturing. The texturing process would still involve an element of conversion, as the matrix does not consist of pure BKT. Some Fe_2O_3 must be added to the mixture to retain the composition near the MPB. The sintering will thus always involve an element of conversion of the templates to the desired structure. In that case, converting the BiT particles to BKT before texturing introduces an extra step and prolongs the process. Based on the results obtained in this study performing RTGG directly without preliminary template conversion is recommended for texturing this system in the future.

5 Discussion

6 Further work

To optimize the synthesis and increase the aspect ratio of the BiT templates, the influence of cooling and heating rates should be further examined.

The conversion of BiT to BKT also needs further inquiries. The mechanism of the whisker formation and the composition of the "free" templates and whiskers should be investigated with the aim of optimizing the conversion process.

As the in-situ conversion of the BiT templates was successful during RTGG, further attempts of texturing of BKT-BF are therefore recommended to be performed by RTGG. However, Fe_2O_3 should be added to the mixture to avoid shifting of the composition towards BKT and keep the textured samples comparable to the untextured reference samples.

The means of orienting the templates in the matrix needs further investigation. Uniaxial pressing at high pressures should be investigated, and if unsuccessful, tape casting may be performed.

Further work is needed in order to assess the effect of crystallographic texture on the electromechanical properties of 0.75BKT-0.25BF.

7 Conclusion

$Bi_4Ti_3O_{12}$ templates have been successfully synthesized with an aspect ratio of 5.0. Investigated parameters were holding time at maximum temperature and cooling rate. It was found that shorter holding times did not influence the particles considerably, while slow cooling rates (180 °C/h) increased the particle size and aspect ratio of the templates.

Molten salt synthesis is not a suitable method for production of plate-shaped $Bi_{0.5}K_{0.5}TiO_3$ templates from $Bi_4Ti_3O_{12}$ precursors. Attempts to convert $Bi_4Ti_3O_{12}$ to $Bi_{0.5}K_{0.5}TiO_3$ gave samples consisting of plate-shaped particles and long whiskers, both of unknown composition. No improvement of the synthesis was detected from increasing the conversion temperature, increasing the holding times at maximum temperature or increasing the amount of molten salt.

Phase pure $0.75Bi_{0.5}K_{0.5}TiO_3$-$0.25BiFeO_3$ powder was synthesized. Textured samples were produced by reactive-templated grain growth, where $Bi_4Ti_3O_{12}$ templates, K_2CO_3 and TiO_2 were added to a matrix of $0.75Bi_{0.5}K_{0.5}TiO_3$-$0.25BiFeO_3$. The precursors were uniaxially pressed to pellets and sintered. Untextured samples were produced as reference. $Bi_4Ti_3O_{12}$ templates were converted to $0.78Bi_{0.5}K_{0.5}TiO_3$-0.22BF during sintering, which is a deviation from the desired composition. The textured samples showed a low degree of texture, possibly due to low density and ineffective orientation of template particles in the matrix. Based on the results in this work uniaxial pressing is not an appropriate method of orienting templates in the matrix.

Both textured and untextured samples did not exhibit ferroelectricity, but were electrically conductive. This may be due to impurities obtained during processing. The effect of crystallographic texture on the electromechanical properties of $0.75Bi_{0.5}K_{0.5}TiO_3$-$0.25BiFeO_3$ needs further investigation.

7 Conclusion

8 Bibliography

1. Haertling, G.H., *Ferroelectric ceramics: History and technology.* Journal of the American Ceramic Society, 1999. **82**(4): p. 797-818.
2. Rodel, J., et al., *Perspective on the Development of Lead-free Piezoceramics.* Journal of the American Ceramic Society, 2009. **92**(6): p. 1153-1177.
3. Jaffe, B., W.R. Cook, and H. Jaffe, *Piezoelectric ceramics*. 1971, London: Academic Press. IX, 317 s. : ill.
4. *Directive 2002/95/EC of the European Parliament and of the Council on the restriction of the use of certain hazardous substances in electrical and electronic equipment.* Official Journal of the European Union, 2003.
5. *Directive 2002/96/EC of the European Parliament and of the Council on waste electrical and electronic equipment.* Official Journal of the European Union, 2003.
6. Leontsev, S.O. and R.E. Eitel, *Progress in engineering high strain lead-free piezoelectric ceramics.* Science and Technology of Advanced Materials, 2010. **11**(4).
7. Messing, G.L., et al., *Templated grain growth of textured piezoelectric ceramics.* Critical Reviews in Solid State and Materials Sciences, 2004. **29**(2): p. 45-96.
8. Morozov, M.I., et al., *Lead-Free Relaxor-Like 0.75Bi(0.5)K(0.5)TiO(3)-0.25BiFeO(3) Ceramics with Large Electric Field-Induced Strain.* Ferroelectrics, 2012. **439**: p. 88-94.
9. Morozov, M.I., M.A. Einarsrud, and T. Grande, *Polarization and strain response in Bi0.5K0.5TiO3-BiFeO3 ceramics.* Applied Physics Letters, 2012. **101**(25).
10. Kim, J.M., et al., *Piezoelectric and Dielectric Properties of Lead-Free (1-x)(Bi0.5K0.5)TiO3-xBiFeO(3) Ceramics.* Ferroelectrics, 2010. **404**: p. 88-92.
11. Ozaki, T., et al., *Microstructures Related to Ferroelectric Properties in (Bi-0.K-5(0).(5))TiO3-BiFeO3.* Japanese Journal of Applied Physics, 2010. **49**(9).
12. Matsuo, H., et al., *Structural and piezoelectric properties of high-density (Bi0.5K0.5)TiO3-BiFeO3 ceramics.* Journal of Applied Physics, 2010. **108**(10).
13. Nye, J.F., *Physical properties of crystals: their representation by tensors and matrices*. 1985, Oxford: Clarendon Press. xvii, 329 s. : fig.
14. Moulson, A.J. and J.M. Herbert, *Electroceramics: materials, properties, applications*. 2003, Chichester: Wiley. XIV, 557 s. : ill.
15. Tilley, R.J.D., *Understanding solids*. 2004, Chichester: Wiley. p. 117, 343-355.
16. Shrout, T.R. and S.J. Zhang, *Lead-free piezoelectric ceramics: Alternatives for PZT?* Journal of Electroceramics, 2007. **19**(1): p. 113-126.
17. Anton, E.M., et al., *Determination of depolarization temperature of (Bi1/2Na1/2)TiO3-based lead-free piezoceramics.* Journal of Applied Physics, 2011. **110**(9).
18. West, A.R., *Basic solid state chemistry*. 1999, Chichester: Wiley. p. 55-59, 362-370.
19. López-Juárez, R., F. González, and M. Villafuerte-Castrejón. *Lead-Free Ferroelectric Ceramics with Perovskite Structure*. Ferroelectrics - Material Aspects 2011 [14.05.2013]; Available from: http://www.intechopen.com/books/ferroelectrics-material-aspects/lead-free-ferroelectric-ceramics-with-perovskite-structure.
20. Aurivillius, B., *Mixed bismuth oxides with layer lattices. 2: Structure of Bi4Ti3O12.* Arkiv for Kemi, 1950. **1**(6): p. 499-512.
21. Kimura, T. and T. Yamaguchi, *Fused salt synthesis of Bi4Ti3O12.* Ceramics International, 1983. **9**(1): p. 13-17.

22. Buhrer, C.F., *Some properties of bismuth perovskites.* Journal of Chemical Physics, 1962. **36**(3): p. 798-&.
23. Wada, T., A. Fukui, and Y. Matsuo, *Preparation of (K0.5Bi0.5)TiO3 ceramics by polymerized complex method and their properties.* Japanese Journal of Applied Physics Part 1-Regular Papers Short Notes & Review Papers, 2002. **41**(11B): p. 7025-7028.
24. Catalan, G. and J.F. Scott, *Physics and Applications of Bismuth Ferrite.* Advanced Materials, 2009. **21**(24): p. 2463-2485.
25. Zhang, J.X., et al., *Large field-induced strains in a lead-free piezoelectric material.* Nature Nanotechnology, 2011. **6**(2): p. 97-101.
26. Rojac, T., M. Kosec, and D. Damjanovic, *Large Electric-Field Induced Strain in BiFeO3 Ceramics.* Journal of the American Ceramic Society, 2011. **94**(12): p. 4108-4111.
27. Selbach, S.M., *Structure, stability and phase transitions of multiferroic BiFeO3*, in *Department of Materials Science and Engineering*2009, Norwegian University of Science and Technology.
28. Kamba, S., et al., *Infrared and terahertz studies of polar phonons and magnetodielectric effect in multiferroic BiFeO3 ceramics.* Physical Review B, 2007. **75**(2).
29. Shvartsman, V.V., et al., *Large bulk polarization and regular domain structure in ceramic BiFeO3.* Applied Physics Letters, 2007. **90**(17).
30. Rojac, T., et al., *Strong ferroelectric domain-wall pinning in BiFeO3 ceramics.* Journal of Applied Physics, 2010. **108**(7).
31. Jones, J.L., B.J. Iverson, and K.J. Bowman, *Texture and anisotropy of polycrystalline piezoelectrics.* Journal of the American Ceramic Society, 2007. **90**(8): p. 2297-2314.
32. Tani, T. and T. Kimura, *Reactive-templated grain growth processing for lead free piezoelectric ceramics.* Advances in Applied Ceramics, 2006. **105**(1): p. 55-63.
33. Yilmaz, H., G.L. Messing, and S. Trolier-McKinstry, *(Reactive) templated grain growth of textured sodium bismuth titanate (Na1/2Bi1/2TiO3-BaTiO3) ceramics - I processing.* Journal of Electroceramics, 2003. **11**(3): p. 207-215.
34. Tani, T., *Texture engineering of electronic ceramics by the reactive-templated grain growth method.* Journal of the Ceramic Society of Japan, 2006. **114**(1329): p. 363-370.
35. Lotgering, F.K., *Topotactical reactions with ferrimagnetic oxides having hexagonal crystal structures. 1*. Journal of Inorganic & Nuclear Chemistry, 1959. **9**(2): p. 113 -
36. Smart, L. and E. Moore, *Solid state chemistry: an introduction*. 2005, Boca Raton, Fla.: Taylor & Francis. 407 s., pl. : ill.
37. Richerson, D.W., *Modern ceramic engineering*. 2006, Boca Raton, Fla.: CRC Press. p. 44, 334-340, 392.
38. Kimura, T., *Molten Salt Synthesis of Ceramic Powders*. Advances in Ceramics - Synthesis and Characterization, Processing and Specific Applications. 2011.
39. Schaak, R.E. and T.E. Mallouk, *Perovskites by design: A toolbox of solid-state reactions.* Chemistry of Materials, 2002. **14**(4): p. 1455-1471.
40. Ranmohotti, K.G.S., et al., *Topochemical Manipulation of Perovskites: Low-Temperature Reaction Strategies for Directing Structure and Properties.* Advanced Materials, 2011. **23**(4): p. 442-460.
41. Zhao, W., et al., *Topochemical synthesis of plate-like Na0.5Bi0.5TiO3 from Aurivillius precursor*. Journal of the American Ceramic Society, 2008. **91**(4): p. 1322-1325.
42. Wu, M.J. and Y.X. Li, *Topochemical synthesis of plate-like Na0.5Bi0.5TiO3 templates from Bi4Ti3O12.* Materials Letters, 2010. **64**(10): p. 1157-1159.

43. Wu, M.J., et al., *Enhanced Electrical Properties of Textured NBBT Ceramics Derived From the Screen Printing Technique.* Ieee Transactions on Ultrasonics Ferroelectrics and Frequency Control, 2011. **58**(10): p. 2036-2041.
44. Seno, Y. and T. Tani, *TEM observation of a reactive template for textured Bi-0.5(Na0.87K0.13)(0.5)TiO3 polycrystals.* Ferroelectrics, 1999. **224**(1-4): p. 793-800.
45. Rise, E., *Synthesis of bismuth titanate templates for tape casting of textured lead-free ferroelectric ceramics. Specialization project.*, in *Department of Materials Science and Engineering*2012, Norwegian University of Science and Technology.
46. Rorvik, P.M., et al., *Influence of volatile chlorides on the molten salt synthesis of ternary oxide nanorods and nanoparticles.* Inorganic Chemistry, 2008. **47**(8): p. 3173-3181.